Structural Lithium Ion Battery Electrolytes

Niklas Ihrner

Doctoral thesis, 2019
KTH Royal Institute of Technology
School of Engineering Sciences in Chemistry, Biotechnology and Health
Department of Fibre and Polymer Technology
Division of Coating Technology
SE-100 44, Stockholm, Sweden

Principal supervisor
Professor Mats Johansson
Co-supervisor
Professor Dan Zenkert

ISBN: 978-91-7873-152-7
ISSN: 1654-1081
TRITA-CBH-FOU- 2019:17
Tryck: US-AB, Stockholm, 2019

Akademisk avhandling som med tillstånd av KTH i Stockholm framlägges till offentlig granskning för avläggande av teknologie doktorsexamen fredagen den 26:e april 2019, kl. 14.00 i sal F3, Lindstedtsvägen 26, KTH, Stockholm. Avhandlingen försvaras på engelska.

Opponent: Professor Daniel Brandell, Uppsala Universitet

In loving memory of Marianne

Abstract

A major challenge in the electrification of vehicles in the transport industry is that batteries are heavy, which reduces their effectiveness in mobile applications. A solution to this is structural batteries, which are batteries that can carry mechanical load while simultaneously storing energy. This can potentially lead to large weight savings on a systems level, since they may allow replacement of load bearing structures with structural batteries. Carbon fibers are suitable for structural batteries because they have superb mechanical properties and readily intercalate lithium ions, i.e. they can be used as electrodes in a lithium ion battery. However, to utilize carbon fibers in structural batteries, a polymer (matrix) is needed to form a composite battery. The polymer is required to have high modulus and high ion transport properties, which are inversely related, to function as an electrolyte. This thesis focuses on the development and characterization of such polymer electrolytes.

The first study was performed on a homogenous polymer electrolyte based on plasticized polyethylene glycol-methacrylate. The influence of crosslink density, salt concentration and plasticizer concentration on the mechanical and electrochemical properties were investigated. Increases in both ionic conductivity and storage modulus were obtained when, compared to non-plasticized systems. However, at high storage modulus (E'>500 MPa) the ionic conductivity ($\sigma<10^{-7}$ S cm^{-1}) is far from good enough for the realization of structural batteries.

In a second study, phase separated systems were therefore investigated. Polymerization induced phase separation (PIPS) via UV-curing was utilized to the produce structural battery electrolytes (SBE), consisting of liquid electrolyte and a stiff vinyl ester thermoset. The effect of monomer structure and volume fraction of liquid electrolyte on the morphology, electrochemical and mechanical properties were investigated. High storage modulus (750 MPa) in combination with high ionic conductivity (1.5 x 10^{-4} S cm^{-1}) were obtained at ambient temperature. A SBE carbon fiber lamina half-cell was prepared via vacuum infusion and electrochemically cycled vs lithium metal. The results showed that both ion transport and load transfer was enabled through the SBE matrix.

In the third study the mechanical and electrochemical properties of the SBE-carbon fiber lamina were investigated and the multifunctional performance was evaluated. A new formulation of SBE, with a small

addition of thiol monomer, were prepared with improved electrochemical and mechanical properties. The mechanical properties of the SBE carbon fiber lamina did not deteriorate after electrochemical cycling. The capacity of the SBE carbon fiber lamina half-cell was 232 ± 26 mAh g^{-1}, at a C/20 charge rate. Furthermore, the lamina displayed multifunctional performance, compared to the monofunctional properties of its constituents.

In the final study, a new curing method was investigated, since UV-curing cannot be used to prepare full-cell carbon fiber composite structural batteries. Thermal curing was investigated to prepare the SBE. The PIPS was not adversely affected by the change in curing method, and the length scale of the phase separation in the SBE was slightly larger compared to UV-cured SBEs. The thermally cured SBEs exhibited improved thermomechanical properties without a reduction in the electrochemical properties. Thermal curing did not affect the electrochemical properties of the SBE carbon fiber lamina, however the type of carbon fiber utilized was found to negatively affect the cycling performance.

Sammanfattning

En stor utmaning i elektrifieringen av fordon inom transportsektorn är batteriers höga vikt, vilket minskar effektiviteten. En lösning på detta problem är strukturella batterier, batterier som kan bära mekanisk last och samtidigt lagra energi. Detta kan potentiellt leda till stora viktbesparingar på systemnivå, genom att ersätta lastbärande delar i konstruktionen med strukturella batterier. Kolfiber har stor potential i utvecklandet av strukturella batterier, de har enastående mekaniska egenskaper samtidigt som de kan interkalera litiumjoner, vilket gör att de kan användas som elektrod i litiumjonbatterier. För att fullt utnyttja kolfiber i strukturella batterier så behövs det en polymermatris för att kunna bilda ett kompositbatteri. Polymeren måste ha både hög modul och hög jonkonduktivitet, egenskaper som tyvärr har en invers relation, för att kunna användas som en elektrolyt. Denna avhandling fokuserar på att utveckla och analysera dessa polymerelektrolyter.

Den första studien genomfördes på homogena polymerelektrolyter baserade på mjukgjorda polyeten glykol metakrylater. Påverkan av tvärbindningstäthet, saltkoncentration och lösningsmedelkoncentration på de mekaniska och elektrokemiska egenskaperna undersöktes. Ökning i både jonkonduktivitet och lagringsmodul, jämfört med icke mjukgjorda system, erhölls. Men vid höga styvheter (E'>500 MPa) var jonkonduktiviteten för låg (σ<10^{-7} S cm^{-1}) för att kunna användas i strukturella batterier.

I andra studien, undersöktes fasseparerade system. Polymerisationsinducerad fasseparation (PIPS) initierad av UV-strålning användes för att framställa strukturella batterielektrolyter (SBE) bestående av vätskeelektrolyt och en härdplast. Påverkan av monomerstruktur och elektrolytvolym på morfologin, de mekaniska och elektrokemiska egenskaperna undersöktes. Hög lagringmodul (E'=750 MPa) i kombination med hög jonkonduktivitet (σ=1,5 x 10^{-4} S cm^{-1}) erhölls vid rumstemperatur. En SBE kolfiberlaminat halvcell tillverkades och cyklades mot litiummetall, som visade att laminatet hade både jonkonduktivitet och lastöverföring.

I den tredje studien undersöktes SBE kolfiberlaminatets mekaniska, elektrokemiska och multifunktionella egenskaper. En ny SBE, där tiol adderades, med förbättrade egenskaper tillverkades. SBE kolfiberlaminatets mekaniska egenskaper förblev oförändrade efter elektrokemisk cykling. Kapaciteten på SBE kolfiberlaminatets halvcell

bestämdes till 232 ± 26 mAh g^{-1}, med en laddningshastighet på C/20. Laminatet uppvisade även multifunktionalitet, jämfört med enskilda beståndsdelarnas monofunktionella egenskaper.

I den sista studien undersöks härdningsmetoden, UV-härdning kan inte användas till att framställa ett helcellskompositbatteri, flera lager kolfiber leder till att UV-ljuset absorberas och ofullständig härdning uppstår. Värmehärdning användes för att framställa SBE. Ingen negativ påverkan på PIPS upptäcktes, däremot upptäcktes att fasseparationen var på en något större längdskala jämfört med UV-härdade prover. De värmehärdade SBE uppvisade bättre termomekaniska egenskaper utan att de elektrokemiska egenskaperna försämrades. SBE kolfiberlaminatet elektrokemiska egenskaper var också oförändrade, dock påverkade den nya typen av kolfiber som användes i denna studie cyklingsprestandadan negativt.

List of appended papers

I. **Improved performance of solid polymer electrolytes for structural batteries utilizing plasticizing co-solvents.**
Niklas Ihrner, Mats Johansson. Journal of Applied Polymer Science 2017, 134 (23), DOI: 10.1002/APP.44917.

II. **Structural lithium ion battery electrolytes via reaction induced phase-separation.**
N. Ihrner, W. Johannisson, F. Sieland, D. Zenkert and M. Johansson. Journal of Materials Chemistry A, 2017, 5, 25652–25659.

III. **Multifunctional performance of a carbon fiber UD lamina electrode for structural batteries.**
Wilhelm Johannisson, Niklas Ihrner, Dan Zenkert, Mats Johansson, David Carlstedt, Leif E. Asp, Fabian Sieland. Composites Science and Technology, 168 (2018) 81–87

IV. **(Submitted manuscript) Bicontinuous electrolytes via thermally initiated polymerization for structural lithium ion batteries.**
Lynn M. Schneider, Niklas Ihrner, Dan Zenkert, Mats Johansson.

Contribution to the papers

I. Performed all of the experimental work and wrote the paper together with M. Johansson.

II. Development, execution and analysis of the SBE. The preparation of the SBE carbon fiber lamina half-cell and the galvanostatic cycling were performed together with W. Johannisson, who performed the mechanical measurement on the SBE carbon fiber lamina half-cell. Wrote the paper together with Mats Johansson.

III. Development, execution and analysis on the SBE. The mechanical and electrochemical preparation and analysis on the SBE carbon fiber lamina was performed by W. Johannisson. The SEM analysis was performed by D. Carlstedt. Contributions to the writing of the paper.

IV. Most of the experimental and analysis work was performed together with L. M. Schneider. L. M. Schneider performed the mechanical and electrochemical measurements on the SBE carbon fiber lamina. Overall analysis of result performed together with L. M. Schneider. Contributions to the writing of the paper.

Other related publications

Temperature-dependent surface nanomechanical properties of a thermoplastic nanocomposite.
Hui Huang, Illia Dobryden, Niklas Ihrner, Mats Johansson, Houyi Ma, Jinshan Pan, Per M. Claesson.
Journal of Colloid and Interface Science, 2017. 494: p. 204-214.

Abbreviations

A	Bisphenol-A-dimethacrylate
AIBN	2,2′-Azobis(2-methylpropionitrile)
B	Bisphenol-A-ethoxylate dimethacrylate
C	2,2′-(ethylenedioxy) diethanethiol
CPE	Composite polymer electrolytes
DMA	Dynamical mechanical analysis
DMMP	Dimethyl methylphosphonate
DMPA	2,2-dimethoxy-2-phenylacetophenone
E’	Storage modulus
EC	Ethylene carbonate
EIS	Electrical impedance spectroscopy
FTIR	Fourier transform infrared spectroscopy
GPE	Gel polymer electrolytes
LiTFS	Lithium trifluoromethanesulfonate
NMP	1-methyl-2-pyrrolidone
NPAL	Tris(N-nitroso-Nphenylhydroxylaminato) aluminum
PAN	Poly(acrylonitrile)
PEG	Poly(ethylene glycol)
PEO	Poly(ethylene oxide)
PET	Poly(ethylene terephthalate)
PIPS	Polymerization induced phase separation
RT-FTIR	Real time fourier transform infrared spectroscopy
SBE	Structural battery electrolyte
SEI	Solid electrolyte interphase
SEM	Scanning electron microscopy
SPE	Solid polymer electrolyte
SR209	Tetraethylene glycol dimethacrylate
SR550	Methoxy polyethylene glycol (350) monomethacrylate
T_{cure}	Curing temperature
T_g	Glass transition temperature
UV	Ultra violet light
Wt.%	Weight percent
σ	Ionic conductivity

Contents

1. Purpose of the study

The purpose of this study was to develop and evaluate polymeric structural lithium ion battery electrolytes with high modulus and high ion conductivity, and to use them for the preparation of structural composite batteries containing carbon fibers.

Carbon fibers can intercalate lithium ions and act as electrodes and current collectors in the battery, while the structural lithium ion battery electrolyte provide ion transport between electrodes and acts as a matrix, binding the composite together. This application places additional requirement on the structural lithium ion battery electrolyte of being suitable for carbon fiber composite manufacturing processes.

The main challenge to overcome, from a polymer electrolyte perspective, is that in polymer electrolytes the modulus and ion transport properties have an inverse relationship. The ion transport is dependent on the chain mobility of the polymer; higher chain mobility leads to higher ionic conductivity. In polymers with high modulus the chain mobility is low, which leads to low ionic conductivity.

2. Introduction

2.1 Context

The ever growing energy demand, partly due to new technologies but foremost due to population growth and an increase in living standard in the third world, requires more efficient ways to store and produce electricity. The United Nations adapted 17 sustainability goals after the 2015 climate meeting in Paris. This work is related to reaching goal 7 (energy), but synergy with other goals can be argued as well.[1]

By adopting existing technologies in new ways, in this case lithium ion batteries and carbon fiber composites, new multifunctional batteries can be envisioned where two properties are combined into one: load bearing with simultaneous energy storage. This would lead to weight savings on a systems level since the structural battery can perform two tasks simultaneously. In an electric vehicle this would mean an increase in driving distance due to a lower overall weight of the vehicle. By improving the driving range, electric vehicles might become more beneficial for a larger part of the population which would also greatly reduce the emission of carbon dioxide, especially in countries like Sweden where the electricity comes mainly from hydro and nuclear power plants.[2] However, it might be even more important for the development of electric commuter airplanes, since in an airplane any weight savings leads to large energy savings during the airplane's lifecycle.

2.2 Lithium ion batteries

Batteries can be divided into two subgroups: primary and secondary batteries, where the latter are rechargeable. They have three primary constituents, electrolyte. positive and negative electrode. The electrodes are where the electrochemical reactions occur, the electrolyte should be electrically insulating and is responsible for transporting ions between the electrodes.

Lithium is desired for use as a negative electrode material due to it being the most electronegative alkali metal (-3.0 V vs SHE), and having

low density (0.534 g cm^{-3}). The low electronegativity if paired with suitable positive electrode materials will lead to high cell voltage, while the low density leads to high specific capacity.

Lithium metal primary batteries were first developed and commercialized during the 1960s and 1970s.[3, 4] However, development of secondary lithium ion batteries was more troublesome, primarily due to lithium dendrite formation during cycling leading to battery short-circuiting and safety concerns.[5-8] This led to the development of intercalation electrodes which were started by Whittingham[9] and later improved by Goodenough et.al. who demonstrated that positive electrode material $LiCoO_2$ cycled stably vs. lithium metal.[10, 11] The same year Rachid Yazami et.al. demonstrated that graphite electrodes could intercalate lithium ions using a solid polymer electrolyte[12], which much later led to the commercialization of secondary lithium ion batteries by Sony in 1991. Since then lithium ion battery technology has progressed and are widely used in portable electronic devices, e.g. smart phones and laptops. In Figure 1 a basic schematic of a lithium ion battery is shown, lithium ions (Li^+) carry charge in the electrolyte and get oxidized/reduced at the electrodes while electrons (e^-) carry charge in the external circuit.

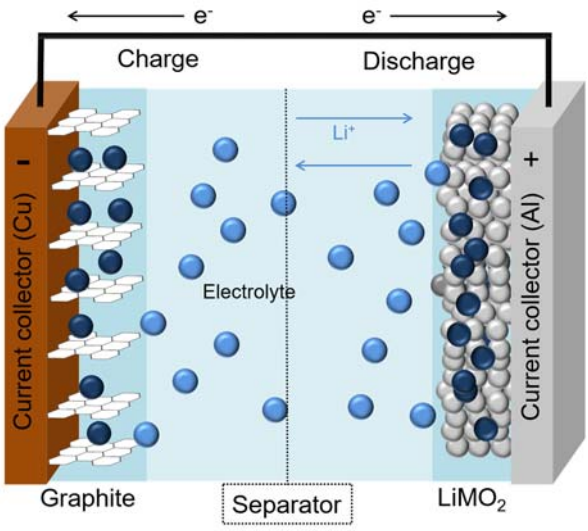

Figure 1 A basic schematic of a lithium ion battery.

The electrode reactions are as following;

Positive electrode: $LiMO_2 \leftrightarrows Li_{1-x}MO_2 + xLi^+ + xe^-$

Negative electrode: $xLi^+ + xe^- + C_6 \leftrightarrows Li_xC_6$

Overall: $LiMO_2 + C_6 \leftrightarrows Li_xC_6 + Li_{1-x}MO_2$

Where M is a metal oxide, e.g. $LiFePO_4$, $LiCoO_2$ or $LiMn_2O_4$, C_6 is graphite, x is a fraction, where 1 means that the battery is fully charged and zero is fully discharged. Reading the reactions from left to right means that the battery is charging, reading from right to left gives the discharge reactions.

2.3 Carbon fibers

Carbon fibers usually have a diameter between 5-10 μm, they are made by carbonization of either pitch (from petroleum) or the synthetic polymer poly(acrylonitrile) (PAN). The carbonization is usually performed between 1000 °C and 3000 °C. After carbonization the fibers are surface treated with a sizing. The sizing serves two purposes; making the fibers easier to handle and increasing the adhesion with polymer resins. The structure of carbon fibers is similar to that of graphite, however they contain more amorphous carbon and the crystalline parts are more disordered. Carbon fibers are state of the art reinforcements in composites. They have low density and excellent tensile properties. The modulus of carbon fibers can range from ultra-high modulus fiber (>500 GPa) to low modulus carbon fiber (100 GPa).[13, 14] Due to the similarity in structure to graphite, studies on using carbon fibers as a negative electrode in lithium ion batteries were initiated in the 90s and are still ongoing.[15-21] It has been shown that carbon fibers readily intercalate lithium-ions, and that fibers made from the precursor PAN have better electrochemical properties and can reach capacities up to 350 mA g^{-1}[16, 17, 21] which is close to the theoretical maximum capacity of graphite (372 mA g^{-1}). Furthermore, carbon fibers are electrically conductive (1000 S cm^{-1})[17], which means that current collectors are not required when using them as an electrode in a battery.

2.4 Structural batteries

The structural battery concept was first introduced in 2004 by Wetzel et.al.[22]. The idea was to reduce the overall weight of a mobile electric device by developing multifunctional batteries that can carry load while simultaneously storing energy. It would then be possible to remove a structural component of the device and replace it with a structural battery, this would reduce the overall weight on a systems level since the battery would now be an integrated part of the device. Since carbon fibers have excellent mechanical properties and can intercalate lithium ions, they can function as a negative electrode in a structural battery. It is also beneficial that they conduct electricity, since they can then act as a current collector at the same time which helps reduce the weight even more. The positive electrode is more of a challenge since carbon fibers without modification can only be used as current collectors. Thus, an active positive electrode material is a prerequisite. In a recently published study by Hagberg et.al.[23], they demonstrate that it is possible to coat carbon fibers with $LiFePO_4$ by electrophoretic deposition. The coated fibers exhibited a capacity of up to 110 mA g^{-1} and displayed good adhesion with an epoxy matrix. However, carbon fibers need a matrix, or in battery terms electrolyte, to fully reach their potential as structural materials. One of the remaining challenges is to develop an electrolyte that is compatible with carbon fibers and that can transport lithium ions while simultaneously transferring loads between the fibers. Liquid electrolyte has traditionally been used in lithium ion batteries due to their high ionic conductivity, however, liquids cannot transfer loads and therefore new electrolyte systems need to be developed, where polymer electrolytes are a promising candidate and are the main focus of this thesis.

2.5 Composites

In load bearing applications, composites are generally built up by a bulk phase, often a polymer, that encloses a reinforcing fibrous phase. e.g. glass, carbon or aramid fibers. The polymer phase (matrix) is responsible for holding fibrous phase together and transferring loads to the fibers, while the fiber phase is responsible for carrying the load. By combining these materials their combined strength masks their individual weaknesses. The fiber phase can be randomly oriented or aligned. Aligned

continuous fibers give rise to the strongest reinforcements.[24] Composites with continuous aligned fibers are anisotropic materials, they will be much stiffer and stronger in the fiber direction compared to the transverse direction (matrix dominated). The earliest known composite shaped by human hands is credited to the ancient Egyptians, they reinforced clay with straw to produce bricks.[25] Nowadays, carbon fibers composites dominate in high performance applications, e.g. race cars, aircrafts, spacecraft and sporting goods. This is due to outstanding mechanical properties combined with their low weight.[24]

2.6 Polymer electrolytes

Research on polymer electrolytes started in the 1970s when it was demonstrated that alkali metal cations could be dissolved and form complexes with poly(ethylene oxide) (PEO).[26, 27] They showed that the lone electron pair on ether oxygen could coordinate to alkali cations and that the conductivity was highly dependent on the temperature and degree of crystallinity of the PEO. A higher temperature and a lower degree of crystallinity lead to higher conductivity. Since then a lot of research has been performed on polymer electrolytes[28-36], which are now often divided into different groups.

Solid polymer electrolytes (SPE), which as the name implies consist solely of solid materials have been pursued mainly due to the potential improvement in safety, chemical stability, thermal stability and dimension stability/flexibility which enable new cell designs. For structural batteries, systems based on crosslinked polymer containing poly(ethylene glycol) (PEG) units have been the most studied.[37-42] The problem with these system, and SPEs in general, is that the ionic conductivity is low especially at higher modulus which is required in structural batteries.

One route to improve the ionic conductivity is to create gel polymer electrolytes (GPE), this can be done by swelling sparsely crosslinked polymers with a suitable liquid electrolyte. Many different polymer backbones have been used for this application, as the polymer itself does not need to be ion conducting, like PEO, PAN, poly(methyl methacrylate) and poly(vinylidene fluoride hexafluoro propylene).[43-57] With GPEs it is possible to reach high ionic conductivity, close to that of liquids (10^{-2} S cm^{-1})[32], nevertheless the increase in ionic conductivity is obtained by sacrificing the mechanical properties which makes GPE unsuitable for

structural batteries where high modulus is crucial. However, combining a SPE with a smaller amount of plasticizing liquid electrolyte could be beneficial and is investigated in Paper I of this thesis. Another solution to the intrinsic problem of the inverse relationship between modulus and ionic conductivity is to create phase separated systems, where one phase is responsible for ion transport and another for mechanical performance. This can be achieved by different paths; the earliest efforts were made by adding inorganic particles as filler in polymer materials forming composite polymer electrolytes (CPE).[58-63] Other approaches have been made by utilizing biomaterials like cellulose and chitosan as reinforcements.[64-68] Although CPE can lead to improvement in both ionic conductivity and modulus, ionic conductivities of 5×10^{-5} S cm^{-1} with a corresponding storage modulus of around 400 MPa has been achieved[68], the incorporation of nano sized fillers could be problematic due to compatibility problems with carbon fibers or composites manufacturing itself. Low viscosity is necessary in composites manufacturing and addition of nano sized fillers is usually followed by significant increases in viscosity.

A more promising approach is phase separated systems consisting of a polymer phase and a liquid electrolyte phase, this has been demonstrated with different chemistries.[69-74] Lodge et.al. demonstrated phase separated membranes plasticized by ionic liquid prepared via PIPS with both high ionic conductivity and storage modulus.[75, 76] The concept of PIPS is interesting for carbon fiber structural batteries since it is possible to start with a solution of low viscosity, which can easily be vacuum infused and then cured into a composite. Paper II-IV are based on the PIPS concept.

2.7 Thermoset polymers

The distinct difference between thermoplastic and thermoset polymers is that thermosets contain crosslinks. The incorporation of crosslinks in a polymer, forming a thermoset, leads to fundamental changes in its properties. Thermosets are insoluble and when heated above their glass transition temperature (T_g) they do not form a melt like thermoplastics; however, like all organic materials they degrade if the temperature is high enough.[77, 78] The properties of thermosets are of course dependent on the chemical structure of their monomers, but they are also dependent on the degree of crosslinking, since the T_g of the monomers increases with

increasing crosslink density. Therefore, the mechanical properties of thermosets can vary greatly, from elastic rubbers (low degree of crosslinking) to very stiff high modulus materials (high degree of crosslinking). Crosslinks, like polymers themselves, can be formed by many different polymerization methods, where free radical polymerization is the prevailing method for commercial materials and the polymerization technique used in this thesis.

2.7.1 Free radical polymerization

Free radical polymerization is a very robust polymerization method, it readily proceeds in the presence ions and other polar compounds, which makes it a suitable reaction mechanism for polymer electrolytes. Most free radical polymerization proceeds by chain-wise propagation, but there are exceptions like thiol-ene system.[79] Two common initiation methods for starting the reaction are thermal and UV initiation. Thermal initiation is widespread in thermoset and composites industries; it is more suitable for curing high T_g polymer systems since vitrification will occur at low temperatures and lead to lower conversion. UV-curing is more rapid, and since it can be performed at ambient temperature the risk of inducing heat related internal stresses is reduced.[80] However, UV-curing requires transparent systems to function properly.

Free radical polymerization of methacrylate

The free radical reaction of methacrylate proceeds via chain-wise propagation, meaning that high molecular weight can be obtained at low conversion.[81] A generalized reaction scheme of initiation and propagation of methacrylate is shown in Figure 2. Both UV and thermal initiation can be used to initiate the reaction. The homo-polymerization of methacrylate is inhibited by oxygen and the polymerization should therefore be performed under inert atmosphere, e.g. argon or nitrogen.

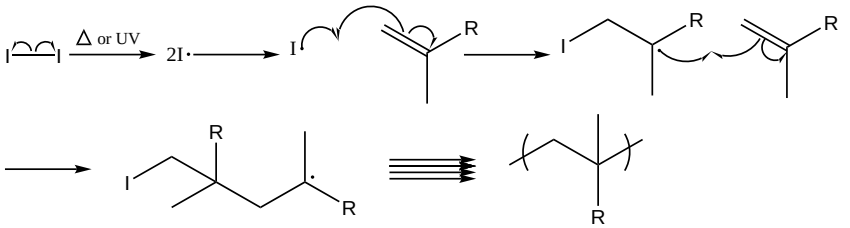

Figure 2 Generalized reaction scheme of initiation and propagation of a methacrylate, where I is the initiator.

Free radical polymerization of thiol-ene

Thiol-ene systems are formed from the reaction of a thiol with an alkene, see Figure 3 for a generalized reaction scheme. Thiol-ene systems proceed via a step-wise propagation mechanism, i.e. high molecular weight is only reached at high conversions. Step-wise mechanisms will also shift the gelation point of the system so that it occurs at higher overall conversion compared to a chain-wise mechanism, which also leads to a more homogenous crosslinked network.[82] This reaction is faster than the homo-polymerization of methacrylate, i.e. if there is an excess of methacrylate monomer, the thiol-ene reaction will dominate until the thiol is depleted.[83, 84] Adding dithiol to a dimethacrylate monomer system will lower the crosslink density, in a thiol-ene reaction the methacrylate is monofunctional, while it is difunctional in the homo-polymerization of methacrylate. A drawback of the thiol-ene system is its high reactivity; it can spontaneously polymerize which means that an inhibitor often has to be added to the system to increase the shelf-life[85].

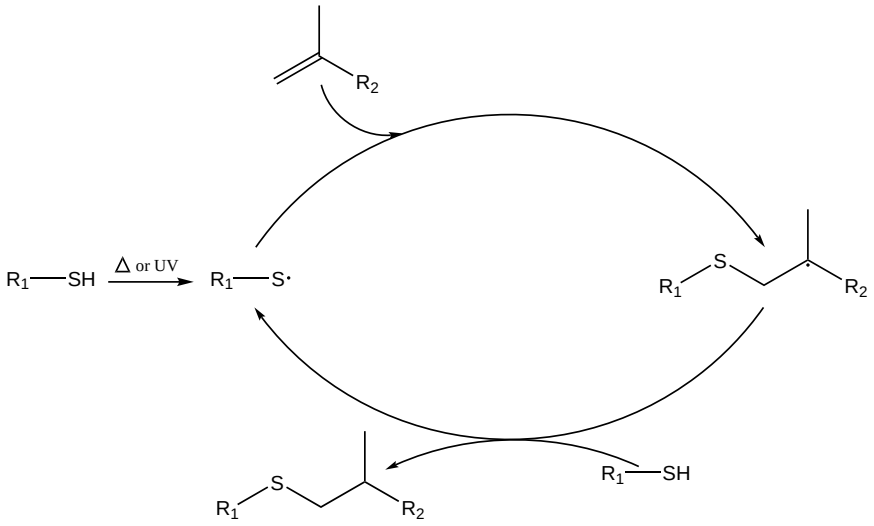

Figure 3 General reaction scheme of a thiol and methacrylate monomer; a thiol-ene reaction.

2.7.2 Vitrification

Vitrification is when a substance transforms into a glass, i.e. a non-crystalline amorphous solid.[86] For high T_g thermoset this can lead to incomplete curing. When the T_g of the forming polymer network reaches the curing temperature (T_{cure}), the forming network starts to enter the glassy state which leads to a reduction in reaction rate, around 3 orders of magnitude. When the T_g of the forming network is much higher than T_{cure} the reaction ceases, the diffusion of monomers/oligomers becomes insignificant and the system is locked.[87]

2.8 Polymerization induced phase separation

PIPS is based on the fact that monomers and the formed polymer can have different miscibility. This makes it possible to choose, e.g. a monomer and a solvent that are miscible upon mixing but during the polymerization a phase separation occurs, the solvent is not miscible with the formed polymer. Using Hansen solubility parameters it is possible to predict systems that can undergo PIPS.[88]

3. Experimental

In this part the experimental details are condensed, for full disclosure see the appended papers.

3.1 Materials

The monomers/oligomers utilized in the thesis, tetraethylene glycol dimethacrylate (SR209; M_n=330 g mol^{-1}), methoxy polyethylene glycol (350) monomethacrylate (SR550; M_n=494 g mol^{-1}) and bisphenol-A-ethoxylate dimethacrylate (B; M_n=540 g mol^{-1} (Paper IV)), were kindly supplied by the Sartomer company. Bisphenol-A-dimethacrylate (A; M=364.43 g mol^{-1}), bisphenol-A-ethoxylate dimethacrylate (B; M_n=540 g mol^{-1} (Paper II-III)) and 2,2′-(ethylenedioxy) diethanethiol (C) were purchased from Sigma-Aldrich.

The solvents and salt used, ethylene carbonate (EC) (98 % Paper I) (99% Paper II-IV), dimethyl methylphosphonate (DMMP) (97%) and lithium trifluoromethanesulfonate (LiTFS) (96%) were purchased from Sigma-Aldrich. 1-methyl-2-pyrrolidone (NMP) were obtained from Labscan.

UV-initiator 2,2-dimethoxy-2-phenylacetophenone (DMPA) was obtained from BASF. Thermal-initiator 2,2′-Azobis(2-methylpropionitrile) (AIBN) and inhibitor tris(N-nitroso-N-phenylhydroxylaminato) aluminum (NPAL) were purchased from Sigma-Aldrich.

Carbon fiber tows (6k) of the type T800H were purchased from Toray and carbon fiber tows (12k) T800S from Toray were provided and spread by Oxeon AB. In Figure 4, the structures of the monomers, solvents and salt are shown.

3.2 Sample preparation

All samples were prepared in a glovebox under Argon atmosphere (<1 ppm H_2O, <1 ppm O_2). The composition of the different sample series is given in the results discussion part of the thesis.

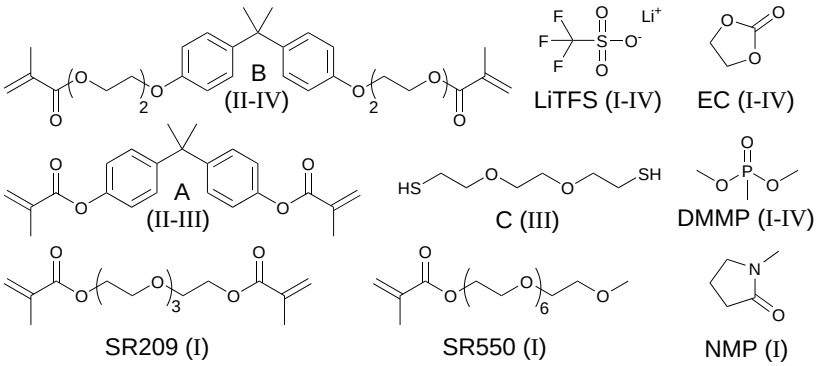

Figure 4 Structure of monomers, solvents and salt used in the study, the roman numerals describes in which Paper the chemical was used.

3.2.1 Solvent and electrolyte preparation

When EC (crystalline at room temperature) is used, a stock solution with its co-solvent was always pre-prepared by heating the mixture to approximately 40 °C forming a homogenous solution. In the phase separated systems (Paper II-IV) a stock solution of liquid electrolyte is prepared by dissolving LiTFS in (EC:DMMP) ((1:1) w/w) until a 1 M solution is obtained.

3.2.2 Polymer electrolyte preparation

The same general procedure has been used to prepare all the polymer electrolyte samples in this thesis, which is as simple as mixing the constituents together in a vial and stirring them by hand (a shaking table was used for samples in Paper I) until a homogenous solution is obtained. When monomer A is used it is necessary to heat the solution (75 °C-80 °C) to melt the monomer. When monomer C (thiol) is used the inhibitor NPAL is also added (0.05 wt.%). The mass of initiator (1 wt.% of the total monomer weight) is the same regardless of which curing method that is employed. When a homogenous solution is obtained, a syringe is used to transfer the solution into an aluminum mold, afterwards the mixture is either UV or thermally cured.

For UV-curing a Blak Ray B100-AP (100 W, 365 nm) Hg UV lamp with an intensity of 5.2 mW cm^{-2} was used as a light source for 4 min inside the glovebox, giving a dose of 1.2 J cm^{-2}.

For thermal curing (Paper IV), a glass slide was put over the mold and clamped which was then vacuum sealed in a pouch. Thermal curing took place in an oven outside the glovebox, samples were cured at three different temperatures, 70 °C, 80 °C and 90 °C.

3.2.3 SBE carbon fiber lamina and half-cell preparation

The same procedure has been used to prepare all carbon fiber lamina half-cells presented in this thesis. The carbon fiber tows (T800H) were spread to reduce their thickness. Copper current collectors are attached to one end of the fiber tow with Electrolube silver conductive paint. The tow is then placed in a vacuum bag with a peel-ply and a distribution medium on a glass plate. The samples were then dried for 12 h in a vacuum oven at 60 °C before being infused (vacuum assisted infusion) with SBE solution (under argon atmosphere). After the infusion the samples were either UV or thermally (Paper IV) cured with the same procedure described in section 3.2.2.

Afterwards, the cured SBE carbon fiber lamina was directly put in a two electrode pouch-cell with lithium metal as counter electrode with a nickel current collector. A Whatman glass microfiber filter was used as separator. Small amounts of liquid electrolyte (1 M LiTFS in EC:DMMP) was used to wet the Whatman filter to ensure ion conduction between electrodes.

3.3 Characterization

3.3.1 Mechanical methods

Dynamical mechanical analysis (DMA)

DMA measurements were performed to evaluate the mechanical properties of the SBEs using a TA Instruments DMA Q800, with the film/tension clamp. Films were clamped with a length of 10–15 mm between the clamps. Samples where always held isothermally for minimum of 10 min before starting the temperature ramp. A ramp rate of 3 °C min^{-1} has been used for all DMA measurements. The amplitude has been set to approximately 0.09 % of the sample length for all samples. Different temperature intervals have been investigated, they can be seen in the results and discussion part of the thesis.

Three-point bending on SBE carbon fiber lamina

The mechanical properties of the SBE carbon fiber lamina was measured with two different instruments. A Deben 300 N micro tester (three-point bending set-up) was used to determine the three elastic properties, longitudinal modulus (E_1) (fiber direction), transverse modulus (E_2), shear modulus (G_{12}) and the 5 strength properties, σ_1 tension and compression (longitudinal), σ_2 tensile and compression (transverse) and the shear strength τ_{12}. Mechanical tests were performed on electrochemically cycled lamina, non-cycled lamina and control samples (SBE without electrolyte). The specimens were thin and proved very challenging to test, especially in the transverse direction with failure loads as low as 1.5 N. Conventional composites measuring methods could not be used, e.g. ASTM D3039. Therefore, an unconventional method was adapted, where the SBE carbon fiber lamina was adhered to a poly(ethylene terephthalate) (PET) film (0.13 mm thick) with a bisphenol A based resin (Reichhold Dion 9102). The mechanical properties of the PET film were determined first, and subsequently the two-layer specimens. The mechanical properties of the SBE carbon fiber lamina was then back-calculated using standard lamina theory.[89] With this method it also became possible to measure the compressive material properties, by inverting the specimen the bending translates to compression in the lamina. To determine the orthotropic stiffness properties, the laminas were tested in longitudinal, transverse and off axis (10°) directions. The in-plane shear modulus G_{12} was obtained from the stiffness of the 10° off-axis samples. The load displacement curves were used to determine the ultimate tensile and compressive strengths, by identifying the first deviation from linearity. This was also selected as the ultimate load, which by using the samples bending stiffness and geometry can be transformed to the ultimate stress. By calculating the shear stress at failure in the 10° off-axis samples the shear strength can be obtained.

An Instron 5567 universal testing machine with a 5 kN load cell was used for pure tension tests in the longitudinal direction to verify the adapted method, the longitudinal and transverse strains were measured with a digital image correlation (DIC) method (GOM Aramis 5M 2016) to calculate the longitudinal modulus E_1 and the major Poisson's ratio (υ_{12}).

3.3.2 Electrochemical methods

Electrical impedance spectroscopy (EIS)

EIS were used to measure the ionic conductivity in the polymer electrolyte films. Samples were measured with a Gamry Series G 750 Potentiostat/ Galvanostat/ ZRA interface together with a four-point electrode setup. The four-point electrode setup utilizes gold wires as electrodes, with two working electrodes (20 mm distance) and two reference electrodes in between them (5 mm distance). The impedance was measured in the frequency range from 300 kHz or 120 kHz (Paper III-IV) to 1 Hz, with an amplitude of 10 mV. The ionic conductivity (σ) was calculated with the following equation;

$$\sigma = l/(R_b \cdot A) \qquad (1)$$

where l is the distance between the reference electrodes (5 mm), R_b is the bulk resistance obtained from the low frequency intercept with the real axis in the Nyquist plot from the EIS measurement, and the cross sectional area (A) of the sample being measured.

Galvanostatic cycling of SBE carbon fiber lamina

The electrochemical capacity was determined by galvanostatic cycling between 2 mV and 1.5 V vs. Li/Li^+. Three different current densities have been employed, 74.4 mA g^{-1} (C/5), 37.2 mA g^{-1} (C/10) and 18.6 mA g^{-1} (C/20). The C-rates (C/5-C/20) are calculated with respect to the theoretical maximum capacity of graphite (372 mA h g^{-1}).

3.3.3 Spectroscopic and microscopic methods

FTIR and RT-FTIR measurements

The conversion of the curing of the polymer electrolytes was measured with FTIR. A PerkinElmer Spectrum 2000 and Spectrum 100 instruments equipped with a single reflection attenuated total reflection (ATR) accessory unit, with a diamond ATR crystal (Golden gate) from Graseby Specac Ltd were used. A resolution of 4 cm^{-1} was chosen and 16 scans were performed on each sample.

RT-FTIR was recorded with the program TimeBased from PerkinElmer (on the Spectrum 100 instrument), 1 scan per 5.7 s with a resolution of 4 cm^{-1} was used. A droplet of SBE solution was put on the heated ATR crystal, with and without carbon fibers, and covered with a glass slide. This was performed at three different temperatures (70 °C, 80 °C, 90 °C).

Scanning Electron Microscope (SEM)

SEM imaging was used to investigate the microstructure of fractured SBE films and SBE carbon fiber laminas. Two different instruments have been used, a Hitachi S-4800 equipped with a cold field-emission electron source and Zeiss Leo Ultra 55 field emission gun scanning electron microscope. Samples where sputter-coated with palladium (Pd) to ensure sufficient conductivity.

A gravimetric analysis was performed when preparing samples for the SEM analysis. Samples were weighed before being immersed in water (removal of LiTFS) and weighed again after being dried in vacuum oven (at 50 °C).

4. Results and discussion

4.1 Homogenous Polymer Electrolytes (Paper I)

The aim of Paper I was to investigate how the addition of plasticizing solvents affects the properties of a thermoset polymer with varying degrees of crosslink density and lithium salt concentration. Could the σ be increased without decreasing the storage modulus (E') by using a plasticizing solvent?

Three different test series were prepared for evaluating the effect of salt concentration, crosslink density and solvent structure.

4.1.1 Curing

All samples obtained full conversion, i.e. no remaining unsaturation could be detected after curing with FTIR analysis, see Figure 5. This means that the difference in sample properties is not due to incomplete curing.

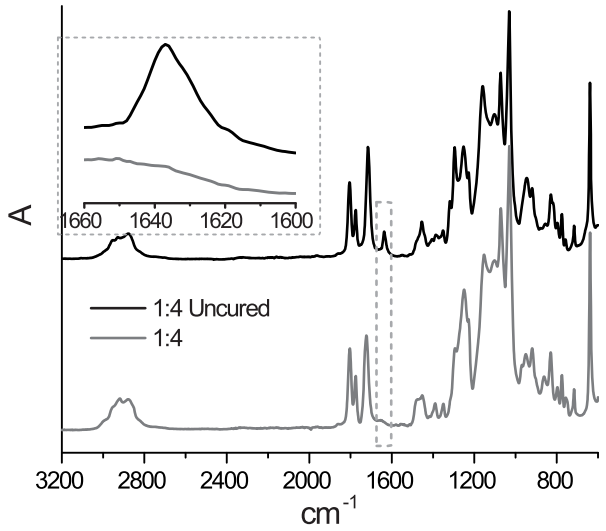

Figure 5 FTIR spectra of sample 1:4, is representative for all samples in the study.

Table 1. Results from the EIS and DMA measurements of samples 1:1-1:4.

Sample	wt.% LiTFS	σ (S cm^{-1})	E'$_{(20\ °C)}$ (MPa)	T_g[a] (°C)	Tan δ_{peak}
1:1	4.4	$8.3 \cdot 10^{-6}$	20	-6	0.33
1:2	8.4	$1.1 \cdot 10^{-5}$	20	-10	0.34
1:3	12.1	$9.3 \cdot 10^{-6}$	20	-12	0.36
1:4	15.5	$5.1 \cdot 10^{-6}$	20	-10	0.39

[a] T_g is assigned as the peak of the Tan δ.

4.1.2 Effect of salt concentration

In Table 1 the results for sample 1:1-1:4 are presented, monomer (SR209 (0.5 g), SR550 (0.5 g)) and solvent (EC (0.15 g), DMMP (0.15 g)) mass are kept constant. Varying the LiTFS content, from 4.4 wt.% to 15.5 wt.%, has no significant effect on the E' above the T_g of the samples. The highest σ is reached for 8.4 wt.% of LiTFS (sample 1:2), more or less LiTFS leads to a decrease in the σ. Since there is no significant difference between the E' and crosslink density of the samples, the decrease is not due to a reduction in chain mobility of the polymer. In a previous study of a similar system without plasticizing solvents, the T_g increases with increasing LiTFS content.[38] The PEG-segments become stiffer when coordinating with lithium ions. This behavior is not exhibited in this system, i.e. the plasticizing solvent hinders these interactions to some degree. One reason for this could be that the plasticizing solvent helps dissolve the LiTFS and also increases the salt dissociation.

4.1.3 Effect of solvent concentration and crosslink density

Two different crosslink densities were investigated, samples 2:1-2:4 (SR209 (0.5 g), SR550 (0.5 g)) and 2:5-2:8 (SR209 (0.9 g). SR550 (0,1 g)), with four different ratios of solvent but the same mass of LiTFS (0.12 g). Increasing the solvent content decreases the E' (Table 2) and it reduces the T_g. The more densely crosslinked samples (2:5-2:8) are more affected by the plasticizing solvent, the reduction in the height of the tan δ is larger compared to samples 2:1-2:4 (Figure 6). The crosslinking density also decreases with increasing solvent content, the volume increases which leads to lower monomer concentration. Overall, the mechanical properties of polymers with high crosslink density are dominated by the

Table 2. Results from the EIS and DMA measurements for samples 2:1-2:8.

Sample	Solvent (wt.%)	σ (S cm^{-1})	E'$_{(20\ °C)}$ (MPa)	T_g[a] (°C)	Tan δ_{peak}
2:1	4	$2.4 \cdot 10^{-7}$	70	11	0.39
2:2	8	$7.6 \cdot 10^{-7}$	50	4	0.36
2:3	15	$4.3 \cdot 10^{-6}$	40	-4	0.37
2:4	26	$3.3 \cdot 10^{-5}$	20	-15	0.34
2:5	4	-	1950	87	0.32
2:6	8	$1.7 \cdot 10^{-8}$	1350	72	0.30
2:7	15	$5.5 \cdot 10^{-8}$	590	47	0.27
2:8	26	$4.5 \cdot 10^{-6}$	240	29	0.22

[a] T_g is assigned as the peak of the Tan δ

crosslinks, chain rigidity and secondary forces have a much larger impact on polymers with low crosslink density or non-crosslinked polymers.

In Figure 7 it is shown that increasing the solvent content decreases the E', which leads to an increase in the σ. In Sample 2:5, no value for the σ could be obtained. Comparing these results to earlier studies performed by Willgert et.al[41], which used the same monomers but without solvents, it can be seen that at lower E' (<30 MPa) a decade higher σ has been reached without a decrease in the E'. The same trend can be seen for higher E' (>200 MPa) as well, although it is lesser in magnitude.

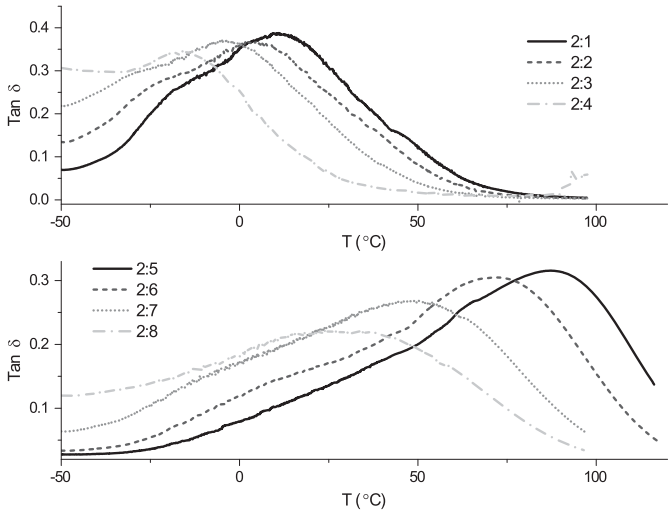

Figure 6 Tan δ vs. temperature, between -50 °C and 120 °C, for samples 2:1-2:8, with varying solvent concentration.

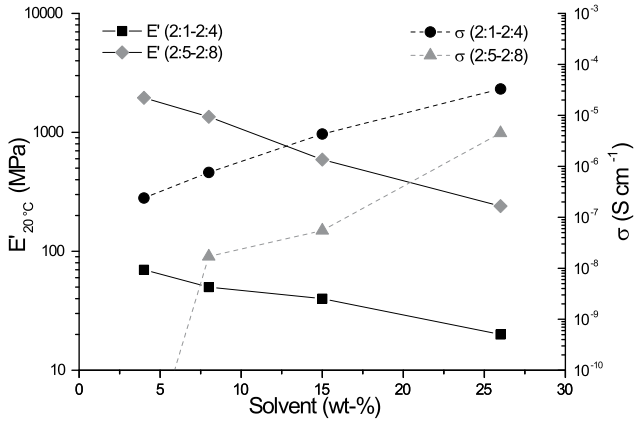

Figure 7 E' and σ plotted vs. solvent content (wt.%). The lines should only be regarded as trend lines.

4.1.4 Effect of solvent composition

In samples 1:2 and 3:1-3:3 (SR209 (0.5 g), SR550 (0.5 g), LiTFS (0.12 g)), four different solvent compositions where investigated. Results are shown in Table 3. The mechanical properties are comparable between the samples, the effect of solvent composition on the mechanical properties are negligible. However, samples containing EC are more heat resistant compared to the samples containing only DMMP or NMP, most likely due to EC's lower vapor pressure. The solvent composition has an effect on the σ; samples with EC have lower σ when compared to the pure co-solvents. The maximum tan δ value increases when EC is used in the solvent mixture, indicating that the interactions between polymer and solvent increase which could have a negative impact on the σ.

Table 3. Results from the EIS and DMA measurements for sample 1:2 and 3:1-3:3.

Sample	Solvent (wt.%)			σ (S cm^{-1})	E'$_{(20\ °C)}$ (MPa)	T$_g$[a] (°C)	Tan δ$_{peak}$
	EC	DMMP	NMP				
1:2	10.5	10.5	0	$1.1 \cdot 10^{-5}$	20	-10	0.34
3:1	0	21.0	0	$1.4 \cdot 10^{-5}$	30	-3	0.32
3:2	10.5	0	10.5	$1.6 \cdot 10^{-5}$	30	-12	0.37
3:3	0	0	21.0	$1.9 \cdot 10^{-5}$	30	-10	0.34

[a] T$_g$ is assigned as the peak of the Tan δ.

Another explanation for this is the higher density of EC, the volume of plasticizing solvent will increase when substituting EC with DMMP or NMP. This could also explain why NMP reaches the highest σ, since it has the lowest density of the three solvents. A concluding observation is that the increase in σ when adding plasticizing solvent is not exclusively due to increased polymer chain mobility, the interaction between solvent and salt also influences the ion transport.

4.2 Phase separated SBE via PIPS (Paper II)

The aim of Paper II was to investigate if it is possible to prepare phase separated SBE with PIPS, where one phase is responsible for mechanical stiffness and strength and the other for ion transport. Is it possible to enhance the electrochemical and mechanical properties and change the relationship between E' and σ?

The system is based on two bisphenol-A-dimethacrylate based monomers (A and B), where monomer B is slightly more polar and leads to polymers with lower crosslink density compared to monomer A. The solvents, EC and DMMP, where selected because of their suitable solubility parameters.[90] Three different monomer compositions with two different liquid electrolyte concentrations were prepared, A/37 wt.%, A/39 wt.%, AB/37 wt.%, AB/39 wt.%, B/37 wt.% and B/39 wt.%. In the AB system the monomer weight ratio is (1:1), the wt.% in the sample name refers to the amount of liquid electrolyte present in the SBE.

4.2.1 Curing performance

The curing performance differs between the monomer compositions (Figure 8), however using 37 or 39 wt.% of liquid electrolyte did not affect the conversion. The highest conversion was reached for system B (95 %). Samples containing monomer A have lower conversions, system AB (82 %) and system A (60 %). The cause of the lower conversions of samples containing monomer A is due to the resulting high T_g of the final SBE films (>150 °C), this results in vitrification effects during curing. Using solely monomer B leads to lower crosslink density in the formed SBE films, and therefore lower T_g, diminishing the vitrification effects[91].

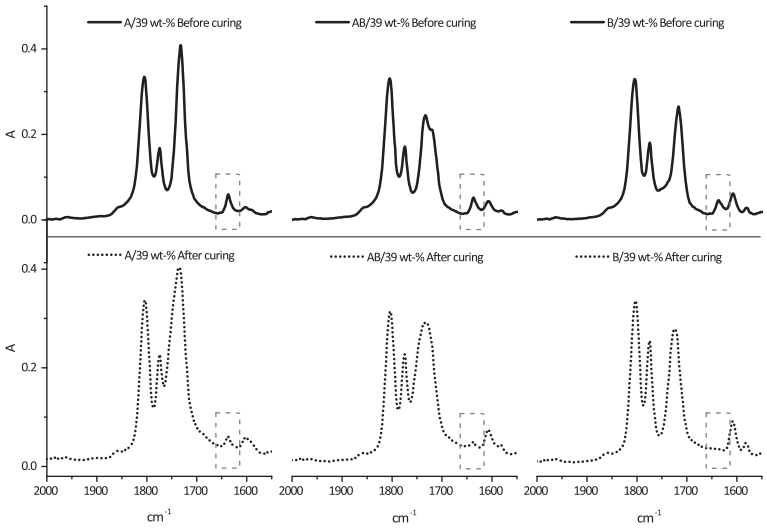

Figure 8 FTIR spectra of samples A/39 wt.%, AB/39 wt.% and B/39 wt.% between 1550 and 2000 cm^{-1}. The circumscribed part shows the vinyl stretching peak at 1637 cm^{-1}.

4.2.2 SBE microstructure

The microstructure of the SBEs are dependent on the PIPS, which is affected by the solubility parameters of the ingoing components, reaction temperature and reaction kinetics. The morphology was studied to see if a correlation could be found for the different sample compositions. The first difference can be seen visually, System B leads to transparent SBE films, while system AB has opaquer films, and system A's films are completely white (Figure 9).

Figure 9 Visual appearance of UV- cured samples containing 37 wt.% liquid electrolyte.

The opacity is mainly related to the scattering of visible light; this means that the phase separation increases in size domain from a nanoscale (system B) to a microscale (system A).

Evaluating the SEM images (Figure 10) validates the visual observation, the phase separation varies in size domain. System B has the smallest pore size, in the range of 50-100 nm, while system A has the largest. The difference in phase separation is attributed to the monomer composition. Monomer B contains, in average, 2 ethylene glycol units between the methacrylate groups, which makes it more compatible with the electrolyte compared to monomer A. This causes the phase separation to be pushed to a later stage in the curing in which the emerging network has a larger obstructive force on the diffusion of the liquid electrolyte.

All samples appear homogenous on a macro scale, i.e. there are no visible gradients in the SBE films. If gradients are present they could have an adverse effect on both the electrochemical and mechanical properties of the SBEs.

The gravimetric analysis (Table 4) revealed that the liquid electrolyte is easily removed, almost completely, by a simple washing and drying step. These results indicate that, since the amount of enclosed liquid electrolyte in the SBE is small or non-existing (system B), a percolating network has been formed in all samples.

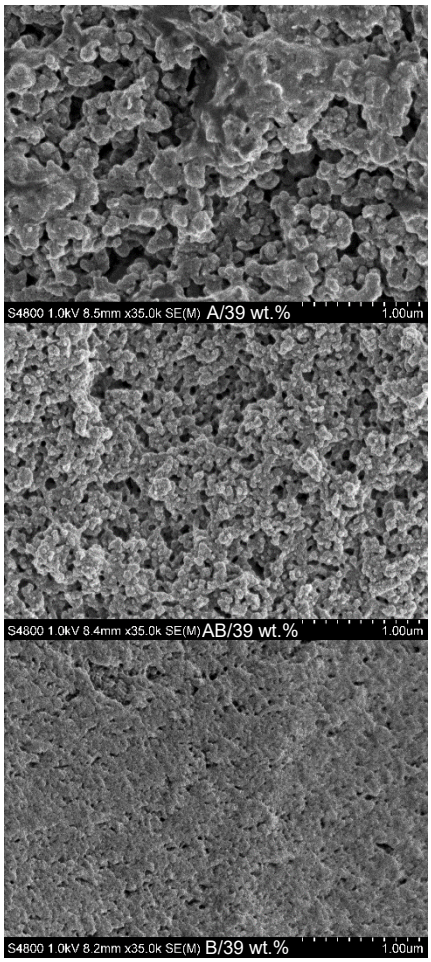

Figure 10 SEM images of sample A/39 wt.%, AB/39 wt.% and B/39 wt.% at 35k magnification.

Table 4. Results from the DMA, EIS and gravimetric analysis.

Sample	σ (S cm^{-1})	E'$_{(25\ °C)}$ (MPa)	T_g[a] (°C)	Sample weight loss after drying (wt.%)
A/37 wt.%	$1.5 \cdot 10^{-4}$	750	-	34
A/39 wt.%	$2.1 \cdot 10^{-4}$	530	-	35
AB/37 wt.%	$1.1 \cdot 10^{-4}$	730	-	37
AB/39 wt.%	$1.9 \cdot 10^{-4}$	550	-	36
B/37 wt.%	$1.2 \cdot 10^{-4}$	380	71	37
B/39 wt.%	$2.0 \cdot 10^{-4}$	360	72	39

[a] T_g selected as Tan $\delta_{peak\ max}$.

4.2.3 Mechanical and electrochemical performance

The mechanical performance varies between the samples. B/37 wt.% and 39 wt.% has a well-defined T_g of 71 °C and 72 °C (Table 4), while samples AB and A (37 and 39 wt.%) have very broad T_g transitions that are higher (Figure 11).

Samples containing monomer A exhibits a behavior typical for highly crosslinked rigid thermosets, there is a gradual decay in the E' with temperature (Figure 12). In sample A/37 and 39 wt.%, which had the lowest conversions, post curing takes place, starting at ca. 100 °C. The main reason for the difference in mechanical properties is the chemical composition: monomer A provides higher crosslink density and is less

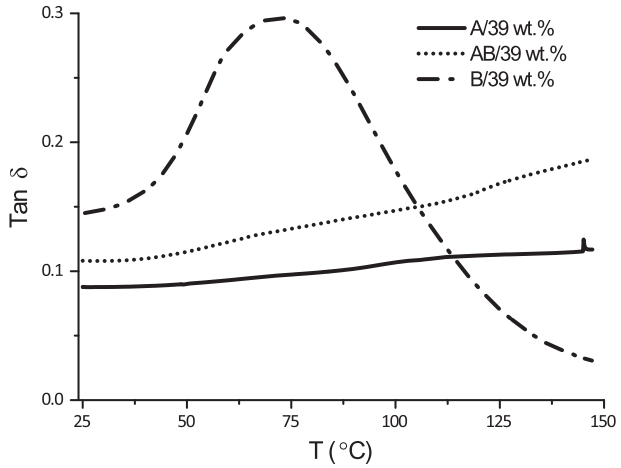

Figure 11 Tan δ vs. temperature for samples with 39 wt.% of liquid electrolyte.

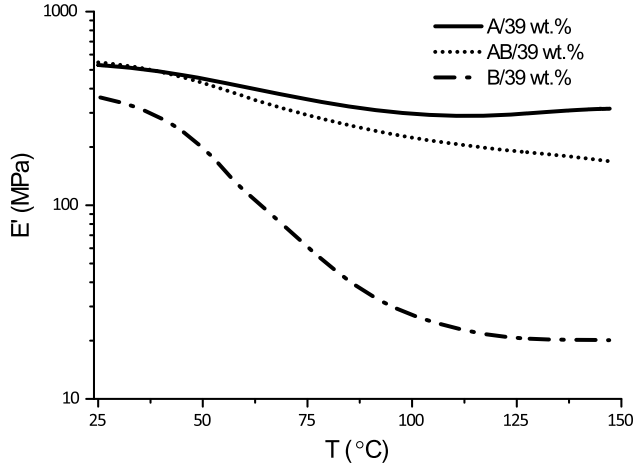

Figure 12 E' vs. temperature for samples with 39 wt.% of liquid electrolyte

aliphatic which give rise to higher E' and T_g. The difference would be even more pronounced if all samples had the same conversion. Another factor that will influence the mechanical properties is if the phase separation is not comprehensive, small amounts of liquid electrolyte left in the polymer phase will act as a plasticizer. Samples B/37 and 39 wt.% are most vulnerable to this effect, however there is no difference in T_g between these samples. If plasticization occurs the T_g should decrease with an increase in liquid electrolyte.

The three different systems exhibit nearly equal σ for the same wt.% of liquid electrolyte (Figure 13), which supports the observation that they are fully phase separated. Additionally, the difference in size domain, between the samples, has no significant effect on the σ. This is reasonable since they all contain the same volume of liquid electrolyte and the polymer phase itself has negligible ion transport properties. In Figure 14 it can be seen how the σ increase with temperature, from room temperature to 100 °C, for the three different systems. The three systems show the same behavior, similar to how traditional liquid electrolyte behaves, which further strengthens the conclusion that the polymer phase has no significant effect on the σ. This is possible due to the fact that the ion transport and mechanical properties are decoupled from each other. In this system the σ is dependent on the intrinsic σ of the liquid electrolyte, its volume fraction and the percolation level of the phase separation.

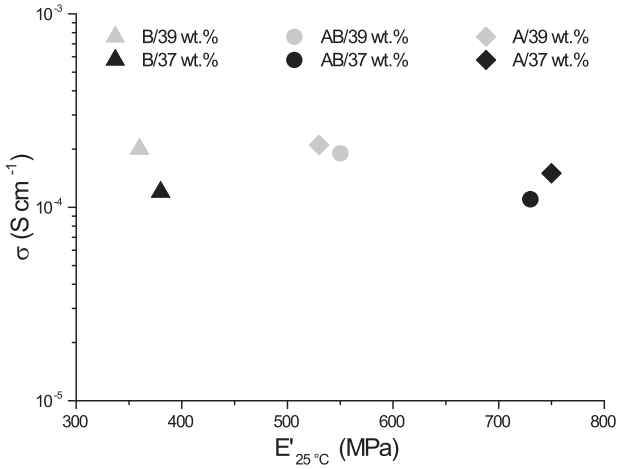

Figure 13 σ vs. E' for system A, AB, and B

At ambient temperature the σ increases almost twofold in all three systems when going from 37 wt.% to 39.wt.% of liquid electrolyte (Table 4). The large increase in σ could indicate that we are close to the percolation threshold when 37 wt.% liquid electrolyte is used, which means that even the small addition of 2 wt.% have a large effect. However, to confirm this a more detailed study would have to be performed. Although the changes in σ are comparable for the three systems the same cannot be said for the E' (Figure 13). The decrease in E'

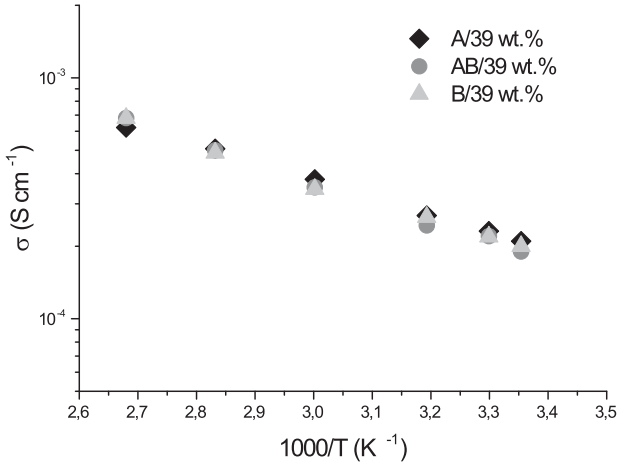

Figure 14 σ vs. 1000/T for samples containing 39 wt.% of liquid electrolyte.

is much larger for sample A/39 wt.% (29 %) and AB/39 wt.% (25 %) compared to sample B/39 wt.% (5 %). In sample A/39 wt.% the increase in brittleness is significant. Samples incorporating monomer B have lower crosslink density and higher conversion, leading to less brittle films.

4.2.4 SBE carbon fiber lamina half-cell

To validate if the SBE could provide multi-functionality in an integrated device, formulation AB/39 wt.% was selected as matrix in a carbon fiber lamina half-cell, and electrochemically cycled. Due to the low viscosity and homogeneity, the formulation solution was easily vacuum infused. This is an important parameter, since it means that already established composite manufacturing techniques can be used for production of structural batteries. The resulting SBE carbon fiber lamina displayed structural integrity. A pouch cell was prepared with lithium foil as a counter electrode, the lithiation and delithiation for the 1st, 2nd and 10th cycle is shown in Figure 15.

The successful cycling of the SBE carbon fiber lamina half-cell establishes that the SBE allows intercalation of lithium ions into the carbon fibers, showing that a layer of the solid polymer phase has not completely formed around the carbon fibers, which would critically

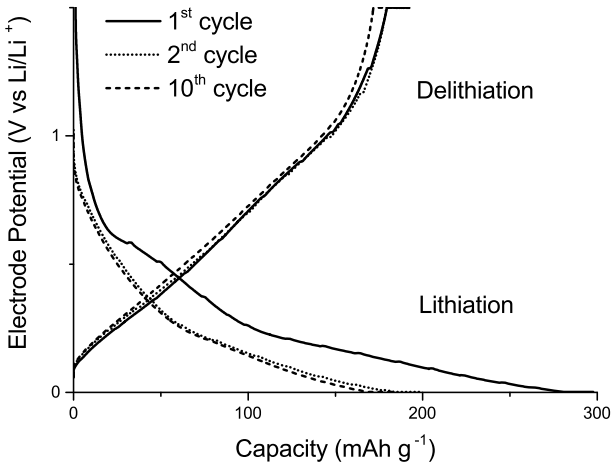

Figure 15 Lithiation and delithiation curves for the 1st, 2nd, and 10th cycle of a SBE carbon fiber lamina prepared with SBE formulation AB/39 wt.% .

inhibit diffusion. The SBE matrix also permits diffusion of lithium ions from the lithium foil through the SBE matrix which further demonstrates that a percolating network of liquid electrolyte is present in the SBE. In the 1st cycle a large decrease in capacity can be seen, which is normally seen in lithium ion batteries. This is a result of the solid electrolyte interphase (SEI) layer forming[92, 93] on the carbon fibers and lithium ions becoming irreversibly trapped in the micro structure of the fibers[21]. The cycling behavior is very similar to previously reported data by M. H. Kjell et.al[17] that used state of the art liquid electrolytes, indicating that there are no large side reactions. Considering that 61 wt.% of the SBE is a rigid thermoset with negligible ion transport properties the capacities are comparable. Mechanical tests on a SBE carbon fiber lamina half-cell in the transverse direction (matrix dominated) gave a transverse elastic modulus of 3.1 GPa, which confirms that there is adhesion between the SBE matrix and the carbon fibers. The electrochemical and mechanical characterization establishes that the SBE in combination with carbon fibers demonstrates multifunctional performance.

4.3 Multifunctional performance of SBE carbon fiber lamina (Paper III)

The aim of Paper III was to further characterize the electrochemical and especially mechanical performance of a SBE carbon fiber lamina half-cell, the multifunctional efficiency is also evaluated. A new SBE system was formulated and evaluated. How does the electrochemical cycling affect the mechanical properties of the lamina?

Compared to the system presented in Paper II, small amounts of dithiol (C) have been added to the system (3.5 wt.%). Six SBE samples and two control samples (without electrolyte) were prepared, AC/39.5 wt.%, AC/40.5 wt.%, AC/Ref, ABC/39.5 wt.%, ABC/40.5 wt.%, BC/37.5, BC/39.5 wt.% and BC/Ref. For all electrochemical and mechanical measurements on SBE carbon fiber lamina (except control samples (AC/Ref)), the same SBE formulation was used, AC/39.5 wt.%.

Table 5. Results from the EIS, DMA and FTIR measurements.

Sample	σ (S cm^{-1})	E'$_{(25\ °C)}$ (MPa)	T_g[a] (°C)	Conversion (%)
AC/39.5 wt.%	$3.2 \cdot 10^{-4}$ ± 5.2 %	690	-	74
AC/40.5 wt.%	$4.9 \cdot 10^{-4}$ ± 3.6 %	640	-	76
AC/Ref	-	2530	-	
ABC/39.5 wt.%	$3.8 \cdot 10^{-4}$ ± 1.3 %	630	-	88
ABC/40.5 wt.%	$4.8 \cdot 10^{-4}$ ± 3.2 %	600	-	88
BC/37.5 wt.%	$1.6 \cdot 10^{-4}$ ± 5.0 %	180	47	98
BC/39.5 wt.%	$3.5 \cdot 10^{-4}$ ± 5.2 %	120	43	98
BC/Ref	-	1400	62	97

[a] T_g selected as the Tan $\delta_{peak\ max}$.

4.3.1 SBE with thiol

The conversions in system AC is roughly 15 % higher compared to system A in section 4.2.1, while the difference is smaller in the other monomer systems (Table 5). The addition of C lowers the crosslink density, and thereby the T_g, which has higher impact with respect to conversion on the high T_g system (A), compared to systems with lower crosslink density (AB, B), which already had fairly high conversions.

The thermomechanical properties of system BC has changed significantly, the E' (at 25°C) of BC/39.5 wt.% is three times lower compared to B/39 wt.% (Table 4) and the T_g has decreased by around 30 °C. The reduction in mechanical properties is not only due to lower crosslink density and the more flexible thioether bond, the systems solubility parameters have also changed and the samples have been slightly plasticized. The T_g decreases with increasing liquid electrolyte concentration (Figure 16), from BC/Ref (62 °C) (no liquid) to BC/39.5 wt. % (43 °C). In a fully phase separated system, i.e. where polymer and liquid does not interact, the T_g would not decrease since it is independent of sample geometry. In contrast the thermomechanical properties are slightly improved in system AC and ABC (Figure 17), which is mainly correlated to the increase in conversion, compared to system A and AB where the conversion was lower. Monomer C will also lead to a more homogenous network which can improve the mechanical performance. At higher temperatures, post curing can be observed which means that the conversion is still limited by vitrification. Monomer C has increased the flexibility of the samples which has made them easier to handle, but also

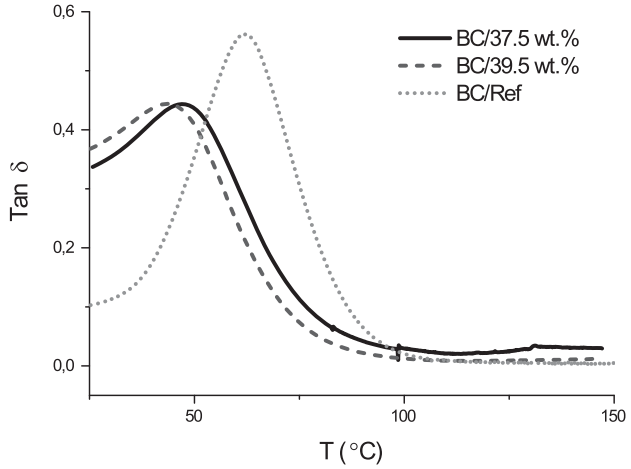

Figure 16 Tan δ vs. temperature for system BC.

increased the maximum achievable loading of liquid electrolyte. In system A, it was not possible to add more than 39 wt.% of liquid electrolyte due to sample fragility at higher concentrations. The σ increases with increasing volume of liquid electrolyte. Monomer C can potentially increase the σ by creating a more homogenous phase separation, which could reduce the tortuosity and thereby decrease the distance ions need to travel. The plasticization occurring in the BC samples does not affect the σ, it is comparable to the σ in system AC and ABC, when the same wt.% of liquid electrolyte is used.

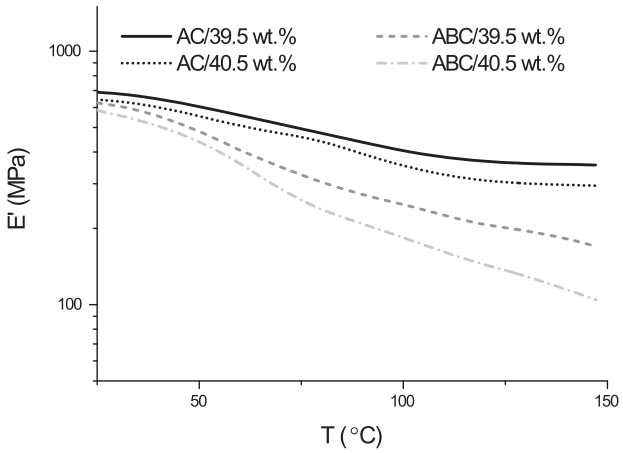

Figure 17 E' vs. temperature for system AC and ABC.

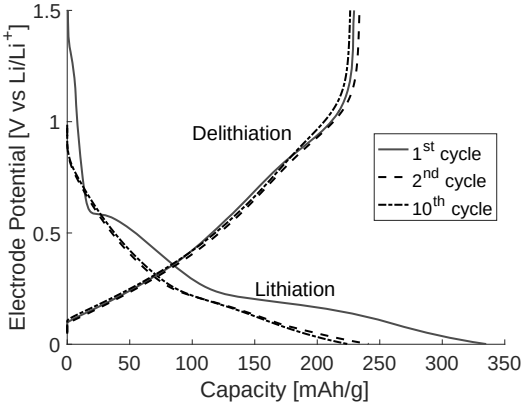

Figure 18 Typical lithiation and delithiation curves for a SBE carbon fiber lamina for the 1st, 2nd and 10th cycle.

4.3.2 Electrochemical testing SBE carbon fiber lamina

Typical results for galvanostatic charging and discharging of a SBE carbon fiber lamina half-cell, with SBE formulation AC/39.5 wt.%, can be seen in Figure 18. They show the same behavior as mentioned in section 4.2.4, but with the exception that the capacity is higher, which is most likely due to the improved performance of the SBE matrix. The average capacity of all half-cells prepared results in a capacity of 232 ± 26 mAh g^{-1}.

4.3.3 Mechanical testing of SBE carbon fiber lamina

The shear modulus (G_{12}) is calculated from the stiffness of the 10°off-axis samples, moduli E_1, E_2 and the value of ν_{12} obtained from tensile testing (Table 6). Data for three longitudinal and three transverse samples from 3-point bending load-displacement experiments are shown in Figure 19. Although the curves are not ideally linear, the asterisk marks where there is a distinct shift in slope and this data is used in the strength calculations. Results from the mechanical tests show that there is no statistical difference in mechanical properties between cycled and non-cycled samples, which is promising as it means there is no mechanical degradation in the SBE matrix when the largest volume changes in the lamina occur.[19]

Table 6. Results from mechanical testing on non-cycled and cycled SBE carbon fiber lamina and the control sample, SBE lamina without electrolyte.

Property, [Unit]	SBE lamina (AC/39.5 wt.%)		Control lamina (AC/Ref)
	Non-cycled	Cycled	
E_1 [GPa]	52 ± 3 (47 ± 5)*	52 ± 2	57 ± 3 (51 ± 6)*
E_2 [GPa]	1.7 ± 0.3	1.9 ± 0.2	3.6 ± 0.3
G_{12} [GPa]	1.5 ± 0.2	1.6 ± 0.2	1.9 ± 0.2
ν_{12} [-]	0.36 ± 0.01*	-	0.44 ± 0.04*
σ_1 tension [MPa]	982 ± 65 (680 ± 88)*	965 ± 134	1046 ± 128 (640 ± 89)*
σ_2 tension [MPa]	12.1 ± 1.6	14.7 ± 3.3	20.0 ± 7.4
σ_1 compression [MPa]	997 ± 59	849 ± 106	1038 ± 130
σ_2 compression [MPa]	11.7 ± 5.2	11.4 ± 1.5	24.3 ± 5.5
τ_{12} [MPa]	13.2 ± 2.4	14.6 ± 3.1	16.5 ± 3.7

* Measured with pure tensile testing, three-point bending was otherwise used.

The control samples (AC/Ref) shows slightly higher moduli and strength, which is expected since the polymer does not contain a porous network. The longitudinal modulus E_1 (fiber direction) values are lower than expected of a carbon fiber UD lamina, this is due to the low volume fraction of carbon fiber (18 %) in both the control and SBE laminae. During manufacture two fairly thick SBE matrix layers are formed on both sides of the spread carbon fibers, which decreases the fiber volume fraction. This can be improved by preparing multiple layers of carbon

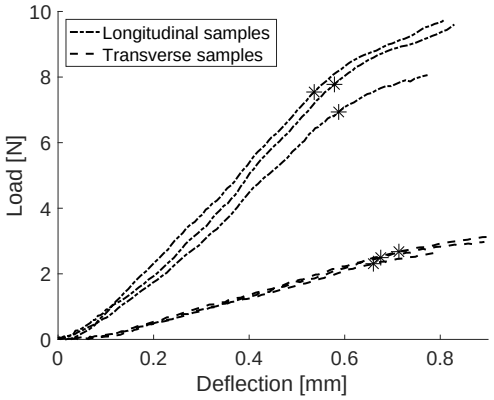

Figure 19 Load displacement curves of non-cycled specimens (transverse and longitudinal) * marks the first deviation from linearity.

fibers, which can double the fiber volume fraction. Increasing the fiber volume fraction is also beneficial for the electrochemical performance, it would reduce the distance between fibers which creates shorter diffusion distances for lithium ions. In Table 6 data marked with an asterisk were tested in pure tensile mode (in the fiber direction), this resulted in a comparable modulus (E_1) which corroborates the 3-point bending experiments. Due to the limitations of the testing setup the strength values should be regarded more as estimates. There are significant differences between the ultimate tensile strength (σ_1) depending on testing method, due to intrinsic test limitations. For the 3-point bending tests the normal stress is uneven over the thickness of the lamina. In the tensile test, the samples are very thin, which makes it difficult to apply an even force, e.g. some fibers break before the whole specimen is fully strained. Nevertheless, the estimated strengths are reasonable since the volume fraction of fibers is low. Importantly, the matrix dominated properties of the lamina (transverse and shear) are comparatively good and do not deteriorate with galvanostatic cycling.

4.3.4 Fiber-matrix interface

In Figure 20, SEM images of non-cycled (a, b), cycled (c, d) and control samples without liquid electrolyte (e, f) are presented. The microstructure of the SBE carbon fiber lamina is comparable to that of the pure SBEs (no thiol) shown in section 4.2.2, i.e. the carbon fibers has no effect on the PIPS. The residual monomer left on both the cycled and non-cycled carbon fibers show that there is adhesion between carbon fiber and SBE (a, c). Furthermore, the expansion of the carbon fibers during cycling does not eradicate the phase separation in the fiber-matrix interface, it remains after cycling (d). From the homogenous control samples (e) it can be seen that the polymer itself adheres to the carbon fibers.

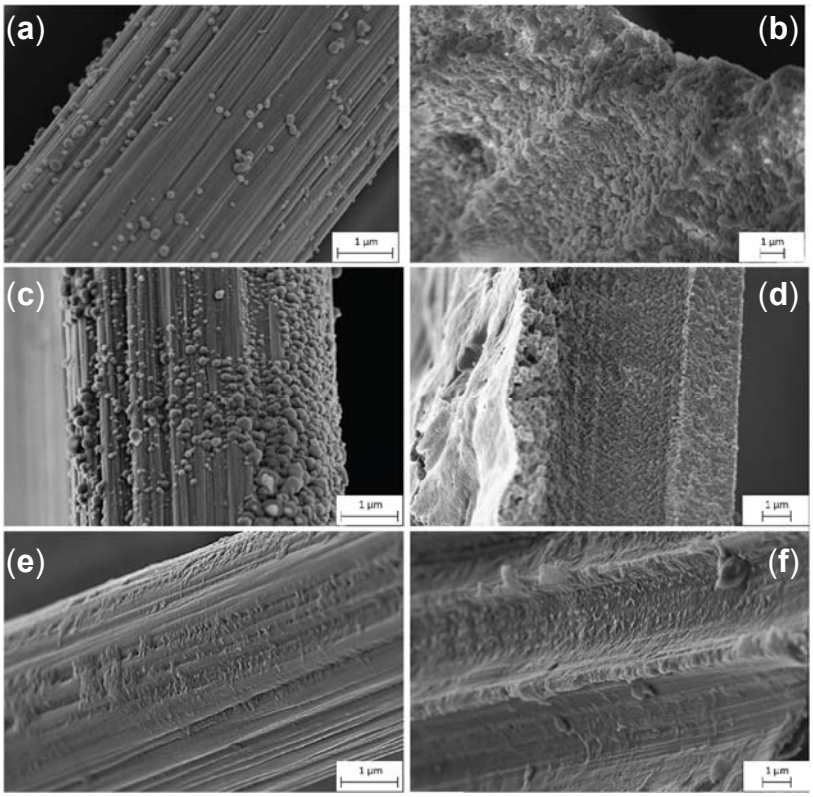

Figure 20 Non-cycled samples, with residual SBE matrix (40k magnification) (a). and SBE matrix with fiber imprint (17.5k magnification) (b). Cycled samples, with residual SBE matrix (40k magnification) (c). and SBE matrix with fiber imprint (20k magnification) (d). Control samples, with residual SBE matrix (40k magnification) (e). and SBE matrix with fiber imprint (20k magnification) (f)

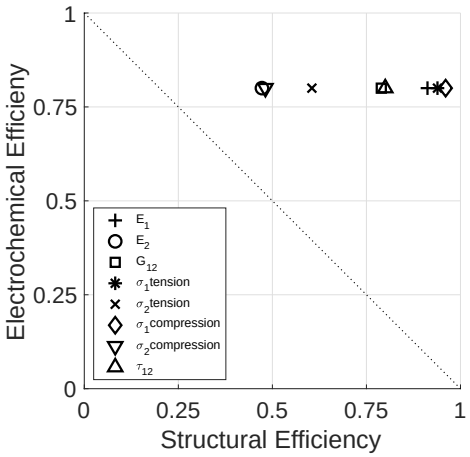

Figure 21 Electrochemical/structural efficiency graph that is normalized to the maximum capacity of the carbon fiber (290 mA g-1)[17] and the respective material properties of the control lamina.

4.3.5 Multifunctional performance

To evaluate the multifunctional performance of the prepared SBE carbon fiber lamina, it is compared to the monofunctional properties of its constituents. In Figure 21, the y-axis is the capacity of the SBE lamina normalized to the maximum capacity of carbon fibers cycled in a liquid electrolyte (290 mAh g^{-1})[17]. On the x-axis the orthotropic material properties of the SBE carbon fiber lamina are normalized to the control sample lamina. Material properties that are located above the diagonal line are considered to demonstrate multifunctional efficiency, i.e. they outperform the separate monofunctional constituents. The result show that all material properties demonstrates good multifunctional efficiency. The analysis was repeated but instead compared to commercial alternatives (Figure 22). The maximum theoretical capacity of graphite (372 mAh g^{-1}) was used to compare the electrochemical efficiency, while a high performance UD carbon fiber lamina with a commercial epoxy prepreg as matrix was used to compare structural efficiency[94]. In this tougher assessment only three mechanical properties show multifunctional efficiency, the longitudinal ultimate tensile and compressive strength (σ_1) and longitudinal modulus (E_1). E_1, as mentioned earlier, can be significantly increased by increasing the volume fraction of fibers. All properties that failed to show

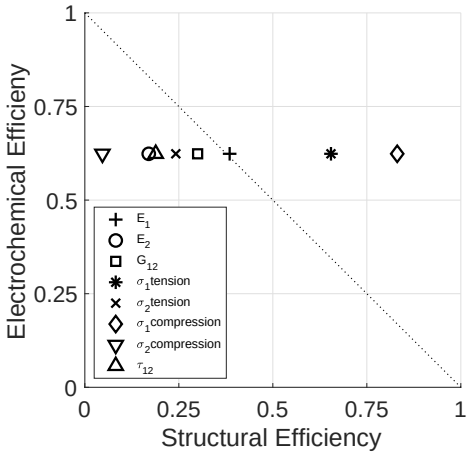

Figure 22 Electrochemical/structural efficiency graph that is normalized to the maximum capacity of the graphite (372 mA g-1) and the material properties of a standard UD carbon fiber epoxy prepreg lamina [93].

multifunctional efficiency are matrix dominated properties, which is expected since a standard epoxy matrix used in carbon fiber composites can have a modulus that is six times higher (E_m=4.1 GPa) which results in an E_2 of around 10 GPa[89]. However, in a composite with several layers of carbon fibers at different angels the fiber dominated properties (E_1) are more important than the matrix dominated (transverse) properties. Hence, by clever engineering the E_1 can compensate for the comparatively poorer matrix dominated properties and will not be detrimental to the overall properties of a multi-angle composite structural battery.

4.4 SBE via thermal PIPS (Paper IV)

The aim of Paper IV was to investigate if the curing method could be changed from UV to thermal curing, where the latter can be used for composite manufacturing and consequently structural battery manufacturing. Can the vitrification effects of high T_g systems observed previously be avoided?

All samples were prepared with the same formulation, monomer B with 39 wt.% of liquid electrolyte. The samples were cured at three different temperatures, 70° C, 80° C and 90° C, with and without carbon

fibers. A UV-cured control sample (B/39 wt.% UV) was also prepared since the monomer used in this study was from a new supplier.

4.4.1 Curing performance

RT-FTIR was used to characterize the curing performance while FTIR was used to determine the conversion. Results from the RT-FTIR show that for curing temperatures of 80° C and 90° C, carbon fibers does not influence the curing (Figure 23). However, at 70 °C the carbon fibers appear to reduce the induction time before the polymerization starts, nevertheless full conversion is reached at the same time. Samples cured at 90 °C show the quickest reaction rate (30 min), while samples cured at 80 °C (60 min) and 70 °C (90 min) are slower. This is mostly due to the rapid increase in half time of the initiator AIBN when the temperature is increased, more radicals are formed at higher temperatures. When curing SBE films and SBE carbon fiber laminae, 15 minutes was added to compensate for the larger setup and additional material that needs to be heated. FTIR was used to determine the double bond conversion of the SBE films that were used for impedance and DMA measurements. Results from Table 7 show that a conversion above 95 % is reached for the 80 °C and 90 °C samples while the 70 °C sample reaches 87 wt.% conversion. The UV-cured control samples had the lowest conversion (85

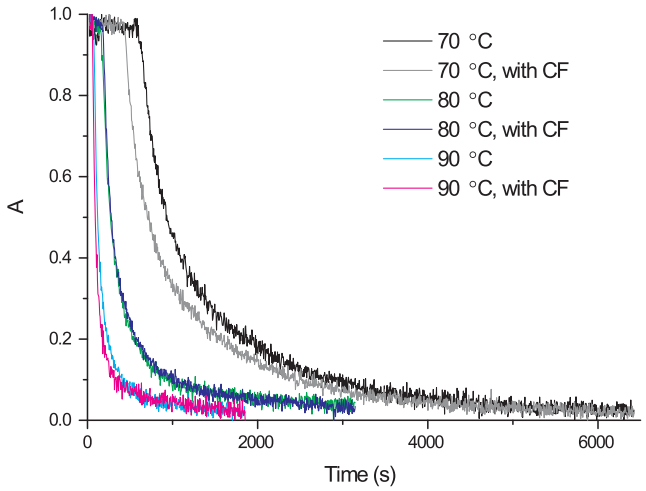

Figure 23 RT-FTIR data of disappearance of the vinyl peak at 1637 cm^{-1} over time. The data has been normalized with respect to the vinyl peak.

Table 7. Results from the FTIR, DMA, EIS and gravimetric analysis of sample B/39 wt.% thermally cured at different temperatures and UV-cured ref. sample.

Sample (°C/UV)	Conversion (%)	$E'_{25\,°C}$ (MPa)	$\sigma_{25°C}$ (S cm^{-1})	Sample weight loss after drying (wt.%)
70	87	490	$1.95 \cdot 10^{-4}$ ± 4.3 %	39.5
80	95	530	$2.00 \cdot 10^{-4}$ ± 7.0 %	38.6
90	96	540	$1.96 \cdot 10^{-4}$ ± 1.3 %	38.1
UV	85	540	$2.02 \cdot 10^{-4}$ ± 3.4 %	38.5

%). The lower conversion of the UV-cured and 70 °C sample is due to vitrification that is reached earlier compared to samples cured at higher temperature. These results differ from the RT-FTIR results, were all thermally cured samples reached equal conversion. This is related to sample geometry effects; the SBE films have a significantly larger volume which leads to distinctly different heat transfer mechanism, which affect the polymerization. For this system a temperature between 80 and 90 °C is suitable for curing.

4.4.2 Microstructure of thermally cured SBE

Visual differences are seen between the UV-cured and thermally cured samples, but also between the thermally cured samples themselves (Figure 24). UV-curing leads to a more transparent SBE film, while the thermally cured samples are more opaque which indicates that the formed discontinuous network is on a larger length scale. Samples cured at 70 °C have a smoother surface compared to samples cured at 80 and 90 °C. One cause for this could be that the 80 and 90 °C curing temperatures give rise to higher thermal stresses, which leads to more cure shrinkage which can create voids at the surface.[95] Viewing the SEM images in Figure 25 it can be confirmed that the UV-cured sample has a phase separation on a smaller length scale than the thermally cured

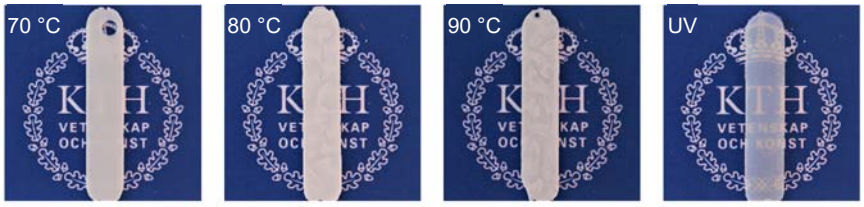

Figure 24 Visual images of B/39 wt.%, thermally cured at 70 °C, 80 °C, 90 °C and a UV-cured ref sample.

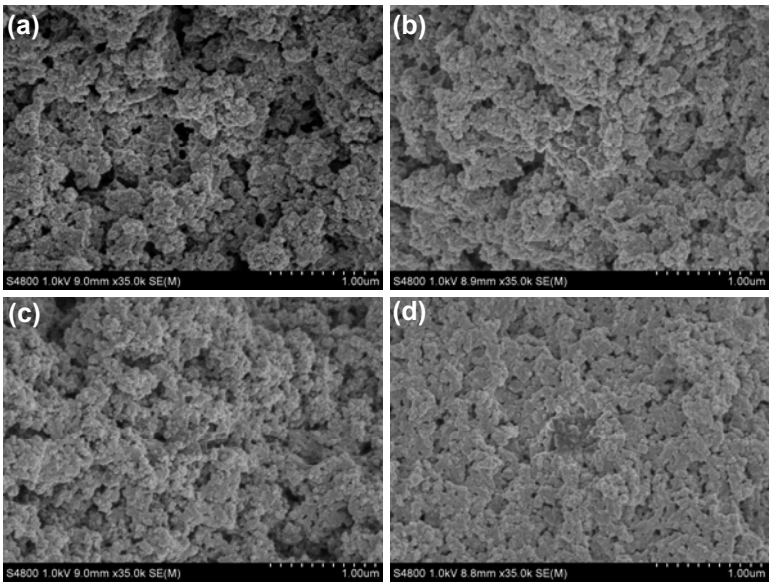

Figure 25 SEM images at 35k magnification of SBE sample B/39 wt.% thermally cured at (a) 70 °C, (b) 80 °C, (c) 90 °C and a UV-cured ref. sample

samples, i.e. the curing method affects the sample morphology. The difference in size domain most likely originates form how the samples are initiated: in UV-curing a high concentration of radicals are formed at the start of the reaction, whereas in thermal curing they are formed more gradually as the temperatures increase. This will lead to different temperature profiles in the specimens which affects both reaction rate and phase separation rate. Comparing the thermally cured sample it can be seen that there is no visible difference in the size domain of the liquid phase, i.e. a 10 or 20°C increase in curing temperature does not affect the size domain of the phase separation. A gravimetric analysis showed that weight loss after washing and drying is comparable to the wt.% of liquid electrolyte used in the specimen formulation (Table 7) which indicates that a percolating network has been formed in all samples.

4.4.3 SBE mechanical & electrochemical performance

From the DMA results it can be seen that the E' of the samples at 25 °C are comparable, except for the 70 °C sample which has a lower modulus (Table 7). However, the main differences between the samples arise with increasing temperature, the 80 °C and 90 °C samples are comparable and

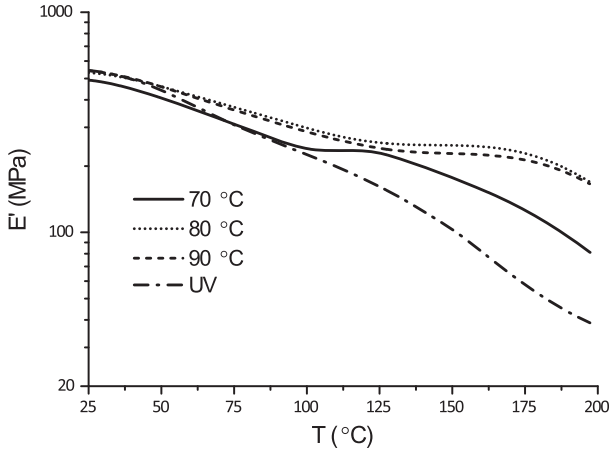

Figure 26 E' vs. temperature for thermally cured sample B/39 wt.% at different curing temperatures and a UV ref. sample

show the highest thermal stability (Figure 26). The difference at higher temperature between the UV and the thermally cured sample at 70 °C is due to the latter undergoing post curing (starts around 100 °C). This behavior is observed in the 80 and 90 °C samples as well but it starts at a higher temperature. The main reason for the difference at higher temperature is the lower conversion, which leads to lower crosslink density and consequently lower thermal stability.

The results from the EIS measurements show that there is no difference in σ between any of the samples, it is around 2 x 10^{-4} S cm^{-1} irrespective of curing method (Table 7). These results are in line with the result from section 4.2.3, i.e. thermal curing is not detrimental to ion transport.

4.4.4 SBE carbon fiber half-cell performance

The SBE carbon fiber lamina was successfully thermally cured at 80 °C. The same type of cell as in section 4.2.4 was prepared. The capacity as a function of the number of electrochemical cycles at three different charge rates is shown in Figure 27. The half-cell exhibits stable cycling but the capacity decreases with increasing charge/discharge rate which is normal for lithium ion batteries, however the magnitude of the decrease in capacity is larger, approximately half the capacity is lost when the charge/discharge rate is doubled. In Figure 28 the potential profiles of the 1st, 2nd and 40th cycle is shown. The potential profiles deviate from

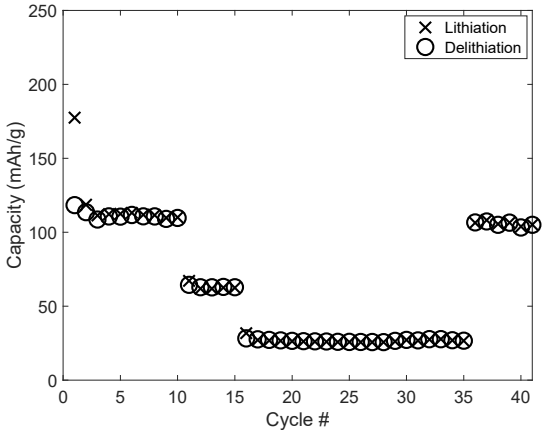

Figure 27 Capacity vs cycle number for three different current densities, 18.6 (16 cycles), 37.2 (5 cycles) and 74.4 mA g^{-1} (20 cycles) of a SBE carbon fiber lamina half-cell prepared by thermal curing (80 °C).

earlier work using the UV-cured systems (section 4.2.4) the capacity is lower and the overpotentials are higher. The main cause of the decrease in performance is due to the new type of carbon fiber used in this study (T800S). In previous work (Paper II and III) the fibers (T800H) were spread by hand, which inevitably leads to variations in the thickness due to the fiber concentration varying along the width of the spread tow. The new fibers are machine spread and more evenly distributed, however the

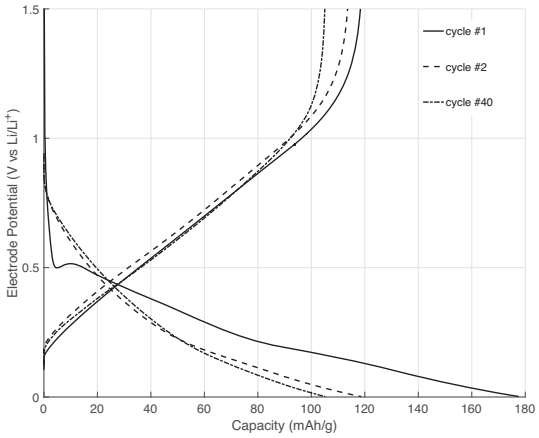

Figure 28 Potential profiles the for the 1st, 2nd and 40th cycle (18.6 mA g^{-1}) of a SBE carbon fiber lamina half-cell prepared by thermal curing (80 °C)

tow contains more fibers which leads to a thicker SBE carbon fiber lamina, about 80 μm compared to the 40-50 μm thick samples obtained previously. The thicker samples struggle with mass-transport limitations and consequently lower capacity for the same charge rates. This is also the reason for the higher overpotentials where the concentration overpotential is most likely the main contributor. The only other difference compared to the carbon fiber used previously is the sizing, which in previous work by Hagberg et.al[21] has been shown to negatively affect the charge rate, this could be another factor that contributes to the poorer performance. The potential profile for 20 cycles of a thermally cured (at 90 °C) SBE carbon fiber lamina half-cell is shown in Figure 29. It was prepared using the T800H fiber tow utilized in Paper II-III, the obtained capacity is comparable to the results in section 4.2.4. This confirms that thermal curing is not detrimental to the electrochemical properties of the lamina half-cell.

The matrix dominated transverse modulus E_2 was measured with the same method as in section 4.3.3 on a thermally cured SBE carbon fiber lamina. The results show an E_2 of 1.3 GPa ±0.1 GPa, which is double the modulus measured with DMA on the pure SBE. This value is lower compared to earlier results (4.2.4, 4.3.3), this is due to the lower intrinsic modulus of the monomer system used in this study.

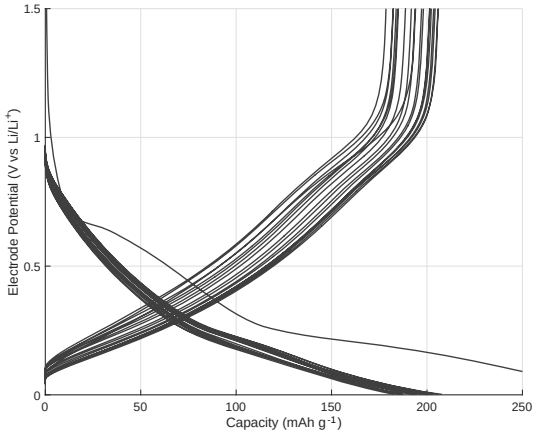

Figure 29 Potential profiles for 20 cycles (18.6 mA g^{-1}) of a SBE carbon fiber lamina half-cell prepared with T800H via thermal curing (90 °C)

The overall results show that thermal curing is a good method for the assembly of SBE carbon fiber laminae, and in the future, full-cell structural composite batteries. Improved conversion and thermo-mechanical properties are achieved compared to UV-curing while there is no difference in ion transport properties.

5. Conclusions

The preparation and evaluation of SBEs for use in the development of structural batteries utilizing carbon fibers as electrodes has been investigated.

The first system investigated was homogenous PEG-methacrylate with different crosslink densities and degree of plasticization. It was found that the mechanical and ion conducting properties of the films can be modified by altering the crosslink density and/or the degree of plasticization. By adding plasticizing solvents, it is possible to significantly increase the σ and still maintain equal or greater E' compared to similar systems without plasticizing solvents. However, even though the overall performance is improved, the relation between E' and σ remains. At higher E' (>500 MPa) the σ is far from good enough for the realization of structural batteries with carbon fibers as electrodes.

This led to the investigation of phase separated systems where a polymer phase is responsible for mechanical strength and a liquid phase responsible for ion transport. Phase separated SBEs were successfully prepared where a σ of 2 x 10^{-4} with a corresponding E' of 550 MPa can be achieved at ambient temperature. Depending on the monomer system used the size domain of the phase separation can be altered from opaque micron-size, to fully transparent nano-sized phase separation. Furthermore, a SBE carbon fiber lamina half-cell is prepared and successfully cycled. After 10 cycles a capacity of 170 mA g^{-1} is obtained. With the multifunctional properties of the prepared phase separated SBE system, carbon fiber composites batteries are one step closer to being realized.

Further investigations on the mechanical properties, and the effect of electrochemical cycling on the SBE carbon fiber lamina half-cell were performed. A new SBE system utilizing small amounts of thiol was produced for this system, which improved electrochemical and mechanical properties. The resulting SBE laminas showed capacities over 200 mA g^{-1} after ten cycles with no decrease in mechanical properties when comparing cycled vs. non-cycled SBE laminae. A longitudinal elastic modulus of 52 GPa is obtained for the SBE-lamina. This value can

be significantly increased by increasing the volume fraction of fibers, which is low (18 %). This could be achieved by improving the manufacturing process. This would also increase the electrochemical performance since diffusion distances would decrease between the fibers in the half-cell. It is also shown that the SBE lamina shows multifunctional efficiency compared to the maximum monofunctional electrochemical and mechanical properties.

The final study was to investigate if the curing method could be changed to thermal curing without reducing the multifunctional performance of the SBE itself and consequently the SBE carbon fiber lamina. The results show that thermal curing has no detrimental effects on the PIPS, with the formed percolating network being on a slightly larger length scale compared to UV-curing. Improvements in both conversion and thermo-mechanical properties are achieved for samples cured at 80 and 90 °C. The cycling performance was also found to be unaffected by the curing method, however the type of fiber used and resulting thickness of the lamina greatly affects the capacity even at slow charge rates.

6. Future work

The aim of the project was to develop SBEs and thereafter use them to prepare carbon fiber composite lithium ion batteries. With the aim in mind, most of the work was directed towards the purpose of demonstrating structural batteries, which led to less time being available for the fundamental understanding of why the SBEs perform as they do, and how to improve the performance of the SBE.

It would be very interesting to modify and formulate new SBE systems, since there is a lot of untapped potential yet to be brought out in the PIPS SBE concept for structural batteries. A detailed investigation on the formation and structure of the phase separation can be prepared simultaneously to give a better understanding of how the phase separation proceeds and which parameters that are important.

The interface between carbon fiber, SEI, and SBE is another important area that needs to be investigated in more detail. The understanding of the interface is crucial for the structural battery function. Here, the sizing on the carbon fibers play an important part, which is a “black box” technology and closely guarded by the industry. Acquiring unsized fibers is difficult, since the manufacturers have to stop the continuous process, before the sizing is applied.

To be able to build a full-cell structural composite battery, studies on the SBEs compatibility with positive electrode materials, e.g. $LiFePO_4$, need to be carried out. How is the electrochemical cycling performance, do unwanted side-reactions arise between electrolyte and $LiFePO_4$?

7. Acknowledgements

First of all, I would like to thank the Swedish Energy Agency (grant # 37712-1), “Structural Batteries for Efficient Vehicles”, for funding the research undertaken in this thesis.

I want to acknowledge professor Mats Johansson for giving me the opportunity and supervising me during my Ph.D. studies, especially for always giving freely of the limited time available for a professor.

I would like to thank all my co-authors for our nice collaborations, being stuck at the glovebox is always more fun when you are there.

The Kombatt research group, is greatly acknowledged for all the interesting technical discussions and the nice atmosphere where there are no “stupid” questions.

I want to acknowledge Linn, Dan, Ross, Lynn and Wille for proofreading this thesis.

I want to thank all the former and current members of ytgruppen. The Senior’s for always trying to improve the already great working environment and always doing your best to take care of us, in all aspects of life. To all the co-workers throughout these four and a half years, it has been a privilege to work with you and get to know you, I miss you already.

I want to thank my family for always being there when it counts, it is a great gift to know that whatever life throws at you there is always a place to call home. I love you all. To Leila, Lennart, Hanna, Madelaine and Stefan, thank you for all the help with Selma, this thesis would not have been finished on time without that help.

To my love Linn. It has “only” been four years since we first met, but we have walked through life together since then. We have experienced wonderful things together, like the day of our marriage and the birth of our daughter Selma. But, we have also experienced some terrible things together, where we found strength in each other. I do not know what the future will bring, however I do know that I want to spend it with you, these years have been the best in my life, I love you and Selma more than my meager talent with words can describe.

8. References

1. Nations, U. *Sustainable Development Goals*. [cited 2019 02-24]; Available from: https://www.un.org/sustainabledevelopment/sustainable-development-goals/.
2. *El och fjärrvärme, Sveriges elproduktion år 2017*. [cited 2019 02-24]; Available from: http://www.energimyndigheten.se/statistik/el-och-fjarrvarme/.
3. Fraioli, A.V.B., W. A. Feldman, A. M., *Composite cathode for voltaic cell*. American Cyanamid Co (Amcy-C).
4. Schneider, A.A. and J. Moser, *Dry,long-life primary element - of lithium/lithium iodine/idine - type,for batteries and heart pacemakers*. Catalyst Res Corp (Catl-C).
5. Selim, R. and P. Bro, *Some Observations on Rechargeable Lithium Electrodes in a Propylene Carbonate Electrolyte*. Journal of The Electrochemical Society, 1974. **121**(11): p. 1457-1459.
6. Rauh, R.D. and S.B. Brummer, *The effect of additives on lithium cycling in propylene carbonate*. Electrochimica Acta, 1977. **22**(1): p. 75-83.
7. Koch, V.R. and J.H. Young, *The Stability of the Secondary Lithium Electrode in Tetrahydrofuran-Based Electrolytes*. Journal of The Electrochemical Society, 1978. **125**(9): p. 1371-1377.
8. Yoshimatsu, I., T. Hirai, and J.i. Yamaki, *Lithium Electrode Morphology during Cycling in Lithium Cells*. Journal of The Electrochemical Society, 1988. **135**(10): p. 2422-2427.
9. Whittingham, M.S., *Electrical Energy Storage and Intercalation Chemistry*. Science, 1976. **192**(4244): p. 1126-1127.
10. Mizushima, K., et al., *LixCoO2 (0<x<-1): A new cathode material for batteries of high energy density*. Materials Research Bulletin, 1980. **15**(6): p. 783-789.
11. Mizushima, K., et al., *LixCoO2 (0<x⩽1): A new cathode material for batteries of high energy density*. Solid State Ionics, 1981. **3-4**: p. 171-174.
12. Yazami, R. and P. Touzain, *A reversible graphite-lithium negative electrode for electrochemical generators*. Journal of Power Sources, 1983. **9**(3): p. 365-371.
13. Chung, D.D.L., *Carbon Fiber Composites*. 1994: Elsevier Science.
14. Donnet, J.B. and R.C. Bansal, *Carbon Fibers, Third Edition*. 1998: Taylor & Francis.
15. Yazami, R., K. Zaghib, and M. Deschamps, *Carbon-Fibers and Natural Graphite as Negative Electrodes for Lithium Ion-type Batteries*. Journal of Power Sources, 1994. **52**(1): p. 55-59.
16. Snyder, J.F., E.L. Wong, and C.W. Hubbard, *Evaluation of Commercially Available Carbon Fibers, Fabrics, and Papers for Potential Use in Multifunctional Energy Storage Applications*. Journal of the Electrochemical Society, 2009. **156**(3): p. A215-A224.
17. Kjell, M.H., et al., *PAN-Based Carbon Fiber Negative Electrodes for Structural Lithium-Ion Batteries*. Journal of The Electrochemical Society, 2011. **158**(12): p. A1455-A1460.
18. Jacques, E., et al., *Impact of electrochemical cycling on the tensile properties of carbon fibres for structural lithium-ion composite batteries*. Composites Science and Technology, 2012. **72**(7): p. 792-798.

19. Jacques, E., et al., *Expansion of carbon fibres induced by lithium intercalation for structural electrode applications*. Carbon, 2013. **59**: p. 246-254.
20. Jacques, E., et al., *The effect of lithium-intercalation on the mechanical properties of carbon fibres*. Carbon, 2014. **68**: p. 725-733.
21. Hagberg, J., S. Leijonmarck, and G. Lindbergh, *High Precision Coulometry of Commercial PAN-Based Carbon Fibers as Electrodes in Structural Batteries*. Journal of The Electrochemical Society, 2016. **163**(8): p. A1790-A1797.
22. Wetzel, E.D., *Reducing weight: Multifunctional composites integrates power, communications, and structure*. AMPTIAC Quarterly, 2004. **8**(4): p. 91-95.
23. Hagberg, J., et al., *Lithium iron phosphate coated carbon fiber electrodes for structural lithium ion batteries*. Composites Science and Technology, 2018. **162**: p. 235-243.
24. Åström, B.T., *Manufacturing of Polymer Composites*. 1997: Chapman & Hall.
25. Delmonte, J., *Historical perspectives of composites*, in *International Encyclopedia of Composites*, S.M. Lee, Editor. 1990, VCH Publishers: New York, NY, USA. p. 335-341.
26. Fenton, D.E., J.M. Parker, and P.V. Wright, *Complexes of alkali metal ions with poly(ethylene oxide)*. Polymer, 1973. **14**(11): p. 589.
27. Wright, P.V., *Electrical conductivity in ionic complexes of poly(ethylene oxide)*. British Polymer Journal, 1975. **7**(5): p. 319-327.
28. Armand, M., *Polymer solid electrolytes - an overview*. Solid State Ionics, 1983. **9–10, Part 2**: p. 745-754.
29. Quartarone, E., P. Mustarelli, and A. Magistris, *PEO-based composite polymer electrolytes*. Solid State Ionics, 1998. **110**(1): p. 1-14.
30. Song, J.Y., Y.Y. Wang, and C.C. Wan, *Review of gel-type polymer electrolytes for lithium-ion batteries*. Journal of Power Sources, 1999. **77**(2): p. 183-197.
31. Manuel Stephan, A. and K.S. Nahm, *Review on composite polymer electrolytes for lithium batteries*. Polymer, 2006. **47**(16): p. 5952-5964.
32. Manuel Stephan, A., *Review on gel polymer electrolytes for lithium batteries*. European Polymer Journal, 2006. **42**(1): p. 21-42.
33. Fergus, J.W., *Ceramic and polymeric solid electrolytes for lithium-ion batteries*. Journal of Power Sources, 2010. **195**(15): p. 4554-4569.
34. Wright, P.V., *Polymer electrolytes—the early days*. Electrochimica Acta, 1998. **43**(10): p. 1137-1143.
35. Meyer, W.H., *Polymer electrolytes for lithium-ion batteries*. Advanced Materials, 1998. **10**(6): p. 439-+.
36. Mindemark, J., et al., *Beyond PEO—Alternative host materials for Li+-conducting solid polymer electrolytes*. Progress in Polymer Science, 2018. **81**: p. 114-143.
37. Willgert, M., et al., *New structural lithium battery electrolytes using thiol–ene chemistry*. Solid State Ionics, 2013. **236**: p. 22-29.
38. Willgert, M., M.H. Kjell, and M. Johansson, *Effect of Lithium Salt Content on the Performance of Thermoset Lithium Battery Electrolytes*, in *Polymers for Energy Storage and Delivery: Polyelectrolytes for Batteries and Fuel Cells*. 2012, American Chemical Society. p. 55-65.
39. Snyder, J.F., E.D. Wetzel, and C.M. Watson, *Improving multifunctional behavior in structural electrolytes through copolymerization of structure- and conductivity-promoting monomers*. Polymer, 2009. **50**(20): p. 4906-4916.
40. Snyder, J.F., R.H. Carter, and E.D. Wetzel, *Electrochemical and Mechanical Behavior in Mechanically Robust Solid Polymer Electrolytes for Use in*

Multifunctional Structural Batteries. Chemistry of Materials, 2007. **19**(15): p. 3793-3801.

41. Willgert, M., et al., *Photoinduced free radical polymerization of thermoset lithium battery electrolytes*. European Polymer Journal, 2011. **47**(12): p. 2372-2378.
42. Nest, J.-F.L., A. Gandini, and H. Cheradame, *Crosslinked polyethers as media for ionic conduction*. British Polymer Journal, 1988. **20**(3): p. 253-268.
43. Sharma, S., et al., *Effect of nano-size fumed silica on ionic conductivity of PVdF-HFP-based plasticized nano-composite polymer electrolytes*. Ionics, 2016. **22**(10): p. 1865-1872.
44. Saikia, D. and A. Kumar, *Ionic conduction in P(VDF-HFP)/PVDF–(PC + DEC)–LiClO4 polymer gel electrolytes*. Electrochimica Acta, 2004. **49**(16): p. 2581-2589.
45. Kelly, I.E., J.R. Owen, and B.C.H. Steele, *Poly(ethylene oxide) electrolytes for operation at near room temperature*. Journal of Power Sources, 1985. **14**(1): p. 13-21.
46. Ito, Y., et al., *Ionic conductivity of electrolytes formed from PEO-LiCF3SO3 complex low molecular weight poly(ethylene glycol)*. Journal of Materials Science, 1987. **22**(5): p. 1845-1849.
47. Nagasubramanian, G. and S. Di Stefano, *12-Crown-4 Ether-Assisted Enhancement of Ionic Conductivity and Interfacial Kinetics in Polyethylene Oxide Electrolytes*. Journal of The Electrochemical Society, 1990. **137**(12): p. 3830-3835.
48. Pitawala, H.M.J.C., et al., *Effect of plasticizers (EC or PC) on the ionic conductivity and thermal properties of the (PEO)9LiTf: Al2O3 nanocomposite polymer electrolyte system*. Journal of Solid State Electrochemistry, 2008. **12**(7): p. 783-789.
49. Cheng, H., et al., *Synthesis and electrochemical characterization of PEO-based polymer electrolytes with room temperature ionic liquids*. Electrochimica Acta, 2007. **52**(19): p. 5789-5794.
50. Watanabe, M., et al., *Ionic conductivity of hybrid films based on polyacrylonitrile and their battery application*. Journal of Applied Polymer Science, 1982. **27**(11): p. 4191-4198.
51. Abraham, K.M. and M. Alamgir, *Li+-Conductive Solid Polymer Electrolytes with Liquid-Like Conductivity*. Journal of The Electrochemical Society, 1990. **137**(5): p. 1657-1658.
52. Appetecchi, G.B., F. Croce, and B. Scrosati, *Kinetics and stability of the lithium electrode in poly(methylmethacrylate)-based gel electrolytes*. Electrochimica Acta, 1995. **40**(8): p. 991-997.
53. Stephan, A.M., et al., *A study on polymer blend electrolyte based on PVC/PMMA with lithium salt*. Journal of Power Sources, 1999. **81–82**: p. 752-758.
54. Egashira, M., et al., *Lithium ion conduction in ionic liquid-based gel polymer electrolyte*. Journal of Power Sources, 2008. **178**(2): p. 729-735.
55. He, R. and T. Kyu, *Effect of Plasticization on Ionic Conductivity Enhancement in Relation to Glass Transition Temperature of Crosslinked Polymer Electrolyte Membranes*. Macromolecules, 2016. **49**(15): p. 5637-5648.
56. Capiglia, C., et al., *Structure and transport properties of polymer gel electrolytes based on PVdF-HFP and LiN(C2F5SO2)2*. Solid State Ionics, 2000. **131**(3–4): p. 291-299.
57. Nguyen, P.-A.T. and J. Snyder, *Multifunctional Properties of Structural Gel Electrolytes*. ECS Transactions, 2008. **11**(32): p. 73-83.
58. Weston, J.E. and B.C.H. Steele, *Effects of inert fillers on the mechanical and electrochemical properties of lithium salt-poly(ethylene oxide) polymer electrolytes*. Solid State Ionics, 1982. **7**(1): p. 75-79.

59. Croce, F., et al., *Nanocomposite polymer electrolytes for lithium batteries*. Nature, 1998. **394**: p. 456.
60. Best, A.S., et al., *Microscopic Interactions in Nanocomposite Electrolytes*. Macromolecules, 2001. **34**(13): p. 4549-4555.
61. Johansson, P., M.A. Ratner, and D.F. Shriver, *The Influence of Inert Oxide Fillers on Poly(ethylene oxide) and Amorphous Poly(ethylene oxide) Based Polymer Electrolytes*. The Journal of Physical Chemistry B, 2001. **105**(37): p. 9016-9021.
62. Croce, F., et al., *Nanocomposite polymer electrolytes and their impact on the lithium battery technology*. Solid State Ionics, 2000. **135**(1): p. 47-52.
63. Croce, F., et al., *Physical and Chemical Properties of Nanocomposite Polymer Electrolytes*. The Journal of Physical Chemistry B, 1999. **103**(48): p. 10632-10638.
64. Azizi Samir, M.A.S., et al., *Plasticized nanocomposite polymer electrolytes based on poly(oxyethylene) and cellulose whiskers*. Electrochimica Acta, 2004. **49**(26): p. 4667-4677.
65. Azizi Samir, M.A.S., et al., *Cellulose nanocrystals reinforced poly(oxyethylene)*. Polymer, 2004. **45**(12): p. 4149-4157.
66. Angulakhsmi, N., et al., *Cycling profile of innovative nanochitin-incorporated poly (ethylene oxide) based electrolytes for lithium batteries*. Journal of Power Sources, 2013. **228**: p. 294-299.
67. Velazquez-Morales, P., J.-F. Le Nest, and A. Gandini, *Polymer electrolytes derived from chitosan/polyether networks*. Electrochimica Acta, 1998. **43**(10): p. 1275-1279.
68. Willgert, M., et al., *Cellulose nanofibril reinforced composite electrolytes for lithium ion battery applications*. Journal of Materials Chemistry A, 2014. **2**(33): p. 13556-13564.
69. Shirshova, N., et al., *Structural supercapacitor electrolytes based on bicontinuous ionic liquid-epoxy resin systems*. Journal of Materials Chemistry A, 2013. **1**(48): p. 15300-15309.
70. Schulze, M.W., et al., *High-Modulus, High-Conductivity Nanostructured Polymer Electrolyte Membranes via Polymerization-Induced Phase Separation*. Nano Letters, 2014. **14**(1): p. 122-126.
71. Shirshova, N., et al., *Composition as a Means To Control Morphology and Properties of Epoxy Based Dual-Phase Structural Electrolytes*. The Journal of Physical Chemistry C, 2014. **118**(49): p. 28377-28387.
72. Greenhalgh, E., et al., *Mechanical, electrical and microstructural characterisation of multifunctional structural power composites*. Journal of Composite Materials, 2015. **49**(15): p. 1823-1834.
73. Gienger, E.B., et al., *Microstructure and multifunctional properties of liquid + polymer bicomponent structural electrolytes: Epoxy gels and porous monoliths*. Journal of Applied Polymer Science, 2015. **132**(42): p. n/a-n/a.
74. Yu, Y., et al., *Co-continuous structural electrolytes based on ionic liquid, epoxy resin and organoclay: Effects of organoclay content*. Materials & Design, 2016. **104**: p. 126-133.
75. Chopade, S.A., et al., *Robust Polymer Electrolyte Membranes with High Ambient-Temperature Lithium-Ion Conductivity via Polymerization-Induced Microphase Separation*. ACS Applied Materials & Interfaces, 2017. **9**(17): p. 14561-14565.
76. McIntosh, L.D., et al., *Evolution of Morphology, Modulus, and Conductivity in Polymer Electrolytes Prepared via Polymerization-Induced Phase Separation*. Macromolecules, 2015. **48**(5): p. 1418-1428.

77. Callister, W.D. and D.G. Rethwisch, *Fundamentals of Materials Science and Engineering: An Integrated Approach*. 2012: Wiley.
78. Sperling, L.H., *Introduction to Physical Polymer Science*. 2005: Wiley.
79. Chanda, M., *Introduction to Polymer Science and Chemistry: A Problem-Solving Approach*. 2006: Taylor & Francis.
80. Decker, C., *Photoinitiated crosslinking polymerisation.* Progress in Polymer Science, 1996. **21**(4): p. 593-650.
81. Chanda, M., *Free Radical Polymerization*, in *Introduction to Polymer Science and Chemistry: A Problem-Solving Approach*. 2006, Taylor & Francis. p. 315-419.
82. Hoyle, C.E. and C.N. Bowman, *Thiol–Ene Click Chemistry*. Angewandte Chemie International Edition, 2010. **49**(9): p. 1540-1573.
83. Lee, T.Y., et al., *Thiol–Allyl Ether–Methacrylate Ternary Systems. Polymerization Mechanism*. Macromolecules, 2007. **40**(5): p. 1466-1472.
84. Hoyle, C.E., A.B. Lowe, and C.N. Bowman, *Thiol-click chemistry: a multifaceted toolbox for small molecule and polymer synthesis.* Chemical Society Reviews, 2010. **39**(4): p. 1355-1387.
85. Hoyle, C.E., T.Y. Lee, and T. Roper, *Thiol–enes: Chemistry of the past with promise for the future*. Journal of Polymer Science Part A: Polymer Chemistry, 2004. **42**(21): p. 5301-5338.
86. Varshneya, A.K., *Fundamentals of Inorganic Glasses*. 2006: Society of Glass Technology.
87. Blair, H.E., Polymer Preprints, 1985. **26**(1): p. 10.
88. Hansen, C.M., *The Three Dimensional Solubility Parameter and Solvent Diffusion Coefficient, Their Importance in Surface Coating Formulation*. 1967, Technical University of Denmark: Danish Technical Press, Copenhagen.
89. Agarwal, B.D. and L.J. Broutman, *Analysis and performance of fiber composites*. 1990: Wiley.
90. Hansen, C.M., *Hansen Solubility Parameters: A User's Handbook, Second Edition*. 2007: CRC Press.
91. Glauser, T., M. Johansson, and A. Hult, *A comparison of radiation and thermal curing of thick composites*. Macromolecular Materials and Engineering, 2000. **274**(1): p. 25-30.
92. Peled, E., *The Electrochemical Behavior of Alkali and Alkaline Earth Metals in Nonaqueous Battery Systems—The Solid Electrolyte Interphase Model.* Journal of The Electrochemical Society, 1979. **126**(12): p. 2047-2051.
93. Aurbach, D., et al., *New insights into the interactions between electrode materials and electrolyte solutions for advanced nonaqueous batteries.* Journal of Power Sources, 1999. **81–82**: p. 95-111.
94. *Performance Composites Ltd, Mechanical Properties of Carbon Fibre Composite Materials, Fibre/Epoxy Resin (120°C Cure).* [cited 2019 03-04]; Available from: http://www.performance-composites.com/carbonfibre/mechanicalproperties_2.asp.
95. Ratna, D., *Handbook of Thermoset Resins: General Introduction to Thermoset Networks*. 2009: iSmithers Rapra Publishing.